

SWIFT BAT SURVEY OF AGNs

J. TUELLER,¹ R. F. MUSHOTZKY,¹ S. BARTHELMY,¹ J. K. CANNIZZO,^{1,2} N. GEHRELS,¹
C. B. MARKWARDT,^{1,3} G. K. SKINNER,^{1,3} AND L. M. WINTER^{1,3}

Received 2007 July 24; accepted 2008 March 17

ABSTRACT

We present the results of the analysis of the first 9 months of data of the *Swift* BAT survey of AGNs in the 14–195 keV band. Using archival X-ray data or follow-up *Swift* XRT observations, we have identified 129 (103 AGNs) of 130 objects detected at $|b| > 15^\circ$ and with significance $> 4.8 \sigma$. One source remains unidentified. These same X-ray data have allowed measurement of the X-ray properties of the objects. We fit a power law to the $\log N$ – $\log S$ distribution, and find the slope to be 1.42 ± 0.14 . Characterizing the differential luminosity function data as a broken power law, we find a break luminosity $\log L_*(\text{erg s}^{-1}) = 43.85 \pm 0.26$, a low-luminosity power law slope $a = 0.84^{+0.16}_{-0.22}$, and a high-luminosity power law slope $b = 2.55^{+0.43}_{-0.30}$, similar to the values that have been reported based on *INTEGRAL* data. We obtain a mean photon index 1.98 in the 14–195 keV band, with an rms spread of 0.27. Integration of our luminosity function gives a local volume density of AGNs above $10^{41} \text{ erg s}^{-1}$ of $2.4 \times 10^{-3} \text{ Mpc}^{-3}$, which is about 10% of the total luminous local galaxy density above $M_* = -19.75$. We have obtained X-ray spectra from the literature and from *Swift* XRT follow-up observations. These show that the distribution of $\log n_{\text{H}}$ is essentially flat from $n_{\text{H}} = 10^{20}$ to 10^{24} cm^{-2} , with 50% of the objects having column densities of less than 10^{22} cm^{-2} . BAT Seyfert galaxies have a median redshift of 0.03, a maximum \log luminosity of 45.1, and approximately half have $\log n_{\text{H}} > 22$.

Subject headings: galaxies: active — gamma rays: observations — surveys

1. INTRODUCTION

It is now realized that most of the AGNs in the universe have high column densities of absorbing material along our line of sight, which significantly changes their apparent properties across much of the electromagnetic spectrum. In many well-studied objects, this material significantly reduces the soft X-ray, optical, and UV signatures of an active nucleus, essentially “hiding” the object. While it is commonly believed that extinction-corrected [O III] can be used as an “unbiased” tracer of AGN activity (Risaliti et al. 1999), there is a large scatter between [O III] and 2–10 keV X-ray flux (Heckman et al. 2005) and between [O III] and BAT flux (Meléndez et al. 2008). We acknowledge that some Compton-thick AGNs are detected in [O III] that cannot be detected in hard X-rays, but Compton-thick AGNs are outside the scope of this paper. Therefore, surveys of AGNs which rely primarily on rest-frame optical and UV studies are very incomplete and have led to misleading results concerning the number, luminosity function, and evolution of active galaxies (e.g., Barger et al. 2005).

While the distribution of column densities is under intensive investigation, it is clear from both X-ray (Tozzi et al. 2006; Cappi et al. 2006) and IR data (Alonso-Herrero et al. 2006) that a large fraction of AGNs have column densities greater than $3 \times 10^{22} \text{ cm}^{-2}$ in the line of sight. Using the Galactic reddening law (Predehl & Schmitt 1995), this is equivalent to $A_V > 13$, making the nuclei essentially invisible in the optical and UV bands. This effect seems to dominate the population seen in deep X-ray surveys (e.g., Barger et al. 2005; Brandt & Hasinger 2005), where a large fraction of the X-ray-selected objects do not have optical counterparts with classical AGN signatures.

There are only two spectral bands in which the nuclear emission is strong and where, provided the column densities are less than $1.5 \times 10^{24} \text{ cm}^{-2}$ (Compton-thin objects), this obscuring material is relatively optically thin. These bands, the hard X-ray ($E > 20 \text{ keV}$) and the IR (5–50 μm), are optimal for unbiased searches for AGNs (Treister et al. 2005). While recent results from *Spitzer* are finding many AGNs via their IR emission, IR selection is hampered by several effects (Barmby et al. 2006; Weedman et al. 2006; Franceschini et al. 2006): (1) the strong emission from star formation, (2) the lack of a unique “IR color” to distinguish AGNs from other luminous objects (Stern et al. 2005), and (3) the wide range in IR spectral parameters (Weedman et al. 2006). Thus, while an IR survey yields many objects, it is very difficult to quantify its completeness and how much of the IR luminosity of a particular galaxy is due to an active nucleus. These complications are not present in a hard X-ray survey, since at $E > 20 \text{ keV}$ virtually all the radiation comes from the nucleus and selection effects are absent for Compton-thin sources. Even for moderately Compton-thick sources, a hard X-ray survey has significant sensitivity, but without an absorption correction the luminosity will be underestimated. Essentially every object more luminous than $10^{42} \text{ erg s}^{-1}$ is an AGN. A hard X-ray survey is thus unique in its ability to find all Compton-thin AGNs in a uniform, well-defined fashion, and to determine their intrinsic luminosity. However, due to the relative rarity of bright AGNs (even the *ROSAT* all-sky survey has only ~ 1 source deg^{-2} at its threshold; Voges et al. 1999), one needs a very large solid angle survey to find the bright, easily studied objects.

With the recent *Chandra* and *XMM* data (e.g., Alexander et al. 2003; Giacconi et al. 2002; Yang et al. 2004; Mainieri et al. 2002, 2005; Szokoly et al. 2004; Zheng et al. 2004; Barger et al. 2001, 2003) there has been great progress in understanding the origin of the X-ray background and the evolution of AGNs. It is now clear that much of the background at $E > 8 \text{ keV}$ is not produced by the sources detected in the 2–8 keV band (Worsley et al. 2005), and is likely to come from a largely unobserved

¹ NASA Goddard Space Flight Center, Astrophysics Science Division, Greenbelt, MD 20771.

² CRESST/Joint Center for Astrophysics, University of Maryland, Baltimore County, Baltimore, MD 21250.

³ CRESST/Department of Astronomy, University of Maryland, College Park, MD 20742.

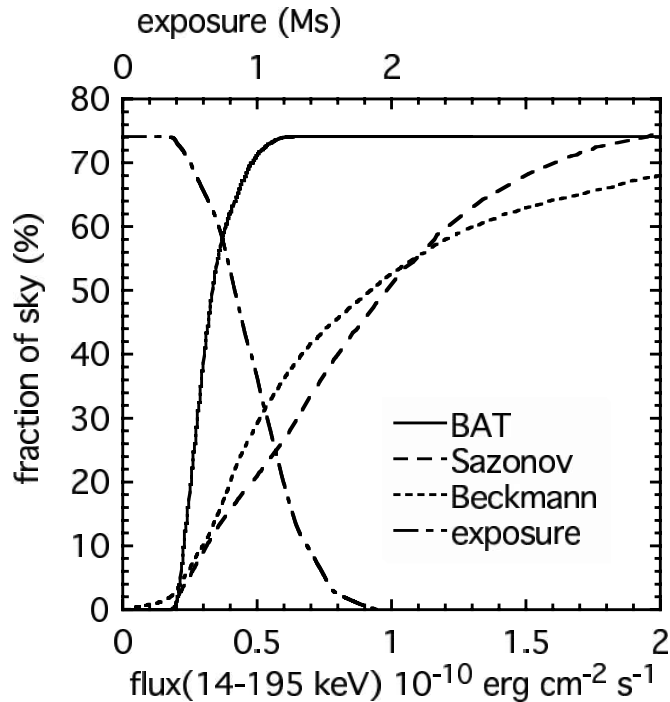


FIG. 1.—Percentage of the sky covered as a function of limiting flux in $\text{erg cm}^{-2} \text{s}^{-1}$ (14–195 keV) and of effective exposure (*upper scale*). As only the sky $|b| > 15^\circ$ is considered here, the maximum value is 74%. The corresponding curves as a function of limiting flux for the analyses of *INTEGRAL* data by Beckmann et al. (2006b) and by Sazonov et al. (2007) are shown for comparison, the flux having been converted assuming a power-law spectrum with index -2 .

population of AGNs with high column density and low redshift $z < 1$. Thus the source of the bulk of the surface brightness of the X-ray background, which peaks at $E \sim 30$ keV (Gruber et al. 1999), is uncertain. The measurement of the space density and evolution of this putative population of highly absorbed AGNs and the derivation of the distribution of their column densities as a function of luminosity and of redshift is crucial for modeling the X-ray background and the evolution of active galaxies. Progress in this area requires both a hard X-ray survey of sufficient sensitivity, angular resolution, and solid angle coverage to find and identify large numbers of sources, *and* follow-up observations with softer X-ray measurements to obtain precise positions and detailed X-ray spectral properties.

Due to a lack of instrumentation with sufficient angular resolution to permit identification of unique counterparts in other wavelength bands and with sufficient solid angle and sensitivity (Krivonos et al. 2005) to produce a large sample, there has been little progress in hard X-ray surveys for over 25 years (e.g., Sazonov et al. 2005, 2007). This situation has been radically changed by the *Swift* BAT survey (Markwardt et al. 2005) and recent *INTEGRAL* results (Beckmann et al. 2006b; Sazonov et al. 2007; Krivonos et al. 2005; Bird et al. 2007) which have detected more than 100 hard X-ray selected AGNs, thus providing the first unbiased sample of Compton-thin AGNs in the local universe.

In this paper we describe results from the first 9 months of the hard X-ray survey using the BAT instrument (Barthelmy et al. 2005) on the *Swift* mission (Gehrels et al. 2004), concentrating on sources with $|b| > 15^\circ$. Above this latitude limit, we have identified all but one of the sources detected at $>4.8\sigma$ with optical counterparts using *Swift* XRT and archival X-ray data. With these same data we have also obtained X-ray spectra. With a median positional uncertainty of $1.7'$ and a sensitivity limit of a few times $10^{-11} \text{ erg cm}^{-2} \text{ s}^{-1}$ in the 14–195 keV band, the BAT data are

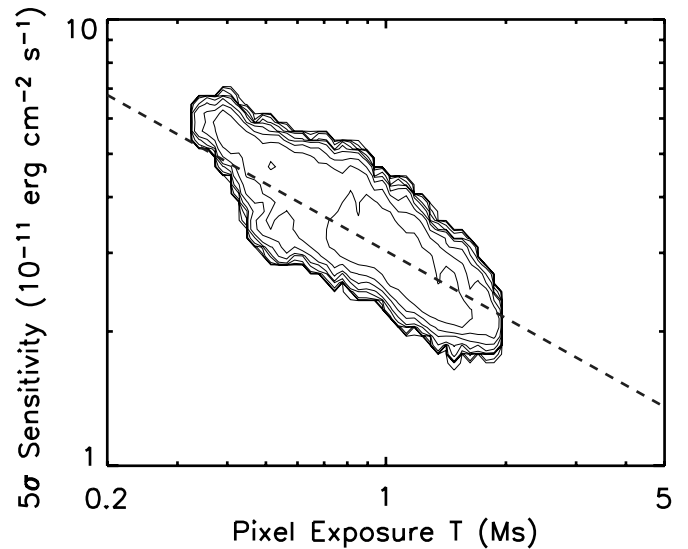


FIG. 2.—BAT survey 5σ sensitivity in the 14–195 keV band for $|b| > 15^\circ$ as a function of exposure. The contours, spaced at logarithmic intervals, indicate the number of pixels ($|b| > 15^\circ$) in the all-sky mosaic with a given exposure and sensitivity. The dashed line indicates the survey sensitivity curve of Markwardt et al. (2005), without adjustment.

about 10 times more sensitive than the previous all-sky hard X-ray survey (*HEAO 1 A-4*; Levine et al. 1984) and the positions are accurate enough to allow unique identifications of nearly all of the sources.

Spectra are characterized by a photon index Γ , where $N(E) \propto E^{-\Gamma}$. Luminosities are calculated using $h_{70} = 1$, $\Omega = 0.3$.

2. BAT SURVEY

The second BAT catalog is based on the first 9 months of BAT data (starting 2005 mid-December) and has several refinements compared to the catalog of the first 3 months of data (Markwardt et al. 2005). The combination of increased exposure, more uniform sky coverage, and improved software has increased the total number of BAT sources by a factor ~ 2.5 .

We show the sky coverage in Figure 1 and the sensitivity of the survey as a function of exposure in Figure 2. There is a loss of sensitivity due to increased noise at low Galactic latitudes from nearby bright sources, and because of spacecraft constraints there tends to be somewhat reduced exposure in directions close to the ecliptic plane. Nevertheless the sensitivity achieved is comparatively uniform.

We have picked a significance threshold of 4.8σ , which, based on the distribution of negative pixel residuals (Fig. 3), corresponds to a probability of ~ 1 false source in the catalog. In Table 1 we show all the sources detected at $>4.8\sigma$ and with $|b| > 15^\circ$. The table also includes sources that have been confidently identified with AGNs but that lie at $|b| < 15^\circ$ or, while having significances less than 4.8σ in the final analysis, have appeared at higher significance in partial or preliminary analyses. Of the 44 AGNs presented in Table 1 of Markwardt et al. (2005), only J1306.8–4023 does not appear in Table 1 of this study. The spectral type is from Véron-Cetty & Véron (2006), and where that is not available, we examined 6dF, SSDS, or our own observations and classified the AGNs. There are seven objects that do not have an optical classification, of which two have not been observed and the remainder do not have optical AGN lines.

We have verified the completeness of our sample by examining the values of V/V_{max} as a function of significance. Above

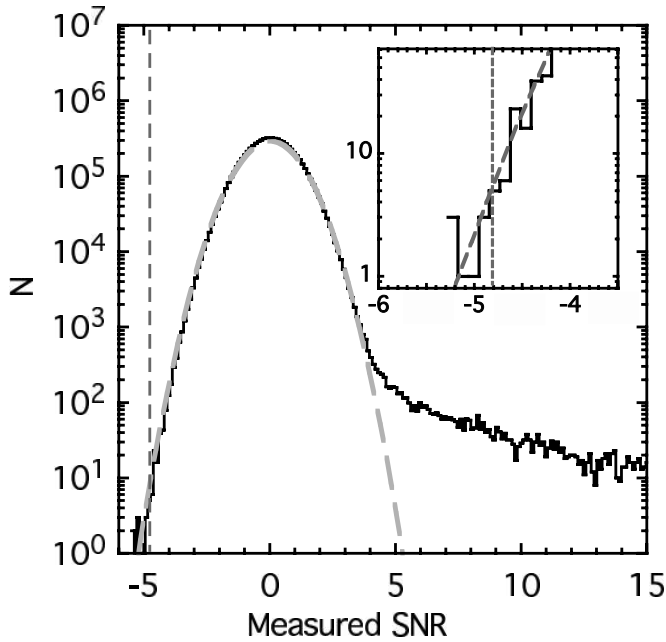


FIG. 3.—Histogram of the pixel values at $|b| > 15^\circ$ in the 9 month survey all-sky map relative to the local estimated noise level. The data closely follow a Gaussian distribution with $\sigma = 1.024$ except for the tail at high positive values due to sources. The insert shows an expansion of the region below $\text{SNR} = -4$. Because of oversampling, more than one pixel corresponds to a single source.

4.8σ detection significance we find a value of 0.5, as expected for a complete sample from a uniform distribution (Fig. 4).

Basing the detection on significance in the total 14–195 keV band is close to optimal for sources with average spectra. We might miss some sources because their spectra are much steeper. However, as shown in Figure 5, there is no apparent correlation between BAT hardness ratio and detection significance and thus we believe that this selection effect is negligible in the present sample.

Because source detection is based on the entire 9 months of data, it is possible that some sources might have been missed if they had been very bright for only a fraction of the observing time. This is confirmed by comparing the present results with those of Markwardt et al. (2005). We found that nine of the Markwardt et al. sources do not lie above our significance threshold of 4.8σ in the 9 months of data.

The accuracy of source positions (Fig. 6) based on the total AGN sample depends on significance; however, at the significance limit of 4.8σ of our survey, the maximum 2σ error circle radius is $\sim 6'$.

3. SAMPLE IDENTIFICATION

BAT is a wide-field (~ 2 steradians) coded-aperture hard X-ray instrument (Barthelmy et al. 2005). During normal operations it usually covers $\sim 60\%$ of the sky each day at < 20 mcrab sensitivity. The BAT spectra were derived from an all-sky mosaic map in each energy bin averaged over 9 months of data beginning on 2004 December 5. The survey was processed using the BAT Ftools⁴ and additional software normalize the rates to on-axis and to make mosaic maps. The intrinsic binning in the BAT survey data product has 80 energy bins but to reduce processing time we used four energy bins for this survey. The energy bin edges are 14, 24, 50, 100, and 195 keV for the 9 month survey, but will be expanded to eight bins in the 22 month survey by dividing each

of the current bins. The energies are calibrated in-flight for each detector using an on-board electronic pulser and the 59.5 keV gamma-ray line and neptunium L-shell X-ray lines from a tagged ^{241}Am source. The average count rate in the map bin that contains the known position of the counterpart was used. Due to the strong correlation of the signal in adjacent map bins of the oversampled coded-aperture image, it is not necessary to perform a fit to the PSF. Each rate was normalized to the Crab Nebula rate using an assumed spectra of $10.4E^{-2.15}$ photons $\text{cm}^{-2} \text{s}^{-1} \text{keV}^{-1}$ for the BAT energy range. Due to the large number of different pointings that contribute to any position in the map, this is a good approximation of the average response. This has been verified by fitting sources known to have low variability and generally produces a good connection to X-ray spectra in sources. Error estimates were derived directly from the mosaic images using the rms image noise in a region around the source of roughly 3° in radius. This is the optimum procedure due to the residual systematic errors of 1.2–1.8 times statistical values in the current BAT mosaics. Analysis of the noise in the images suggests that the variations in noise are small on this scale. Analysis of negative fluctuations shows that the noise is very well fit by a Gaussian distribution and that this normalization is very accurate on average. All fitting of the BAT data was performed on this normalized data using a diagonal instrument response matrix. This procedure correctly accounts for instrumental systematics in sources with spectral indices similar to the Crab. While there may be significant systematic errors for sources with spectra that are much flatter than the Crab, this is not a significant problem for any of the sources presented in this paper.

We first attempted to identify the BAT sources using archival X-ray, optical, and radio data. The typical high Galactic latitude BAT source is a bright (2MASS J -band magnitude > 13) and nearby ($z < 0.1$) galaxy. While the counterpart is often a *ROSAT* or radio source, this is not a reliable indicator. In particular we found little or no correlation between the BAT counting rates and the *ROSAT* all-sky survey fluxes (Fig. 7), making it difficult or impossible to utilize the *ROSAT* data to consistently identify the sources. An examination of random positions suggests this type of source rarely falls in a BAT error circle. While this approach was fruitful, we found a significant number of objects with either no obvious counterpart or multiple possible counterparts, due to clustering. We have followed up with *Swift* XRT all but one of the BAT sources in the second catalog that did not have evident identifications with previously known AGNs, or that did not have archival X-ray measurements of absorption column n_{H} from *XMM*, *ASCA*, *Chandra*, or *BeppoSAX*. We find that if the *Swift* XRT exposure is on the order of 10 ks or greater, we have a high probability of identifying an appropriate candidate. We define an appropriate candidate as one which is within the BAT 2σ error contour and whose X-ray flux is commensurate with the BAT detection. Because of the possibility of source variability and of the low time resolution possible with the BAT data (~ 2 weeks per significant data point) we require only that the X-ray flux is consistent with an absorbed power law model that has a flux within a factor of 10 of that predicted from the BAT detection. A detailed analysis of the variability of the BAT data is presented in Beckmann et al. (2006b) and a comparison of the XRT and other data in Winter et al. (2008).

We have based our identifications on observations in the harder, 2–10 keV, part of the XRT band to minimize the probability of a false identification. A *Swift* XRT detection limit of 0.001 counts s^{-1} , or 10 total counts (0.5–10 keV) in a 10 ks exposure, corresponds to a 0.5–10 keV flux of about 3.7×10^{-14} erg $\text{cm}^{-2} \text{s}^{-1}$ for an unabsorbed source or to 6.3×10^{-14} erg $\text{cm}^{-2} \text{s}^{-1}$ for one

⁴ See http://heasarc.nasa.gov/ftools/ftools_menu.html.

TABLE 1
SWIFT SURVEY TABLE

| No. | Swift Name ^a | ID ^b | R.A. ^c (deg) | Decl. ^c (deg) | >15 ^o d | SNR | f_{BAT}^e | z | $\log L_x^c$ (erg s ⁻¹) | $\log \eta_{\text{H}}^c$ (cm ⁻²) | Ref. ^f | Complex ^g | Type ^h | Note ⁱ | J (mag) | f_{ROSAT}^j | Rate ^{i,k} |
|---------|---------------------------------|-------------------------|----------------------------|-----------------------------|--------------------|-------|--------------------|----------|--|---|-------------------|----------------------|-------------------|-------------------|--------------|----------------------|---------------------|
| 1..... | SWIFT J0042.9-2332 | NGC 235A | 10.7200 | -23.5410 | y | 4.47 | 3.2 | 0.022229 | 43.56 | 23.00 | 1 | y | Sy 2† | | 10.58 | 0.024 | |
| 2..... | SWIFT J0048.8+3155 ¹ | Mrk 348 | 12.1964 | 31.9570 | y* | 13.00 | 9.5 | 0.015034 | 43.68 | 23.32 | 2 | y | Sy 2 | | 11.24 | 0.009 | |
| 3..... | SWIFT J0059.4+3150 | Mrk 352 | 14.9720 | 31.8269 | y* | 4.90 | 3.7 | 0.014864 | 43.27 | 20.75 | 3 | | Sy 1 | | 12.49 | 0.615 | |
| 4..... | SWIFT J0114.4-5522 | NGC 454 | 18.5946 | -55.3986 | y | 4.54 | 2.3 | 0.012125 | 42.88 | 22.95 | 1 | y | Sy 2 | 33 | 13.98 | | |
| 5..... | SWIFT J0123.9-5846 ¹ | Fairall 9 | 20.9408 | -58.8057 | y* | 8.90 | 4.7 | 0.04702 | 44.39 | 20.36 | 4 | | Sy 1 | | 11.85 | 3.350 | |
| 6..... | SWIFT J0123.8-3504 ¹ | NGC 526A | 20.9766 | -35.0654 | y* | 8.20 | 5.2 | 0.019097 | 43.63 | 22.30 | 4 | y | Sy 1.5 | | 11.60 | 0.123 | |
| 7..... | SWIFT J0134.1-3625 | NGC 612 | 23.4906 | -36.4933 | y* | 4.89 | 3.2 | 0.029771 | 43.81 | 23.70 | 5 | y | Gal/Radio | 34 | 11.68 | | |
| 8..... | SWIFT J0138.6-4001 ¹ | ESO 297-018 | 24.6548 | -40.0114 | y* | 9.03 | 4.9 | 0.025201 | 43.85 | 23.84 | 1 | y | Sy 2 | | 9.18 | | |
| 9..... | SWIFT J0201.0-0648 | NGC 788 | 30.2769 | -6.8155 | y* | 8.37 | 5.9 | 0.013603 | 43.39 | 23.48 | 6 | y | Sy 2 | | 10.02 | | |
| 10..... | SWIFT J0209.7+5226 | Mrk 1018 | 31.5666 | -0.2914 | y* | 5.31 | 3.5 | 0.04244 | 44.17 | 20.53 | 1 | | Sy 1.5 | | 11.60 | 0.360 | |
| 11..... | SWIFT J0214.6-0049 | LEDA 138501 | 32.3929 | -0.4425 | y* | 5.13 | 3.9 | 0.0492 | 44.34 | 21.18 | 1 | | Sy 1 | | 11.60 | 0.752 | |
| 12..... | SWIFT J0214.6-0049 | Mrk 590 | 33.6398 | -0.7667 | y* | 5.67 | 3.7 | 0.02638 | 43.77 | 20.43 | 7 | | Sy 1.2 | | 10.71 | 2.689 | |
| 13..... | SWIFT J0216.3+5128 | 2MASX J02162987+5126246 | 34.1243 | 51.4402 | | 4.93 | 3.6 | | | 22.25 | 1 | | Galaxy† | 35 | 14.27 | | |
| 14..... | SWIFT J0218.0+7348 | [HB89] 0212+735 | 34.3784 | 73.8257 | | 4.27 | 2.6 | 2.367 | 48.05 | 23.38 | 1 | | BL Lac | | | 0.044 | |
| 15..... | SWIFT J0228.1+3118 | NGC 931 | 37.0603 | 31.3117 | y* | 8.56 | 7.3 | 0.016652 | 43.66 | 21.65 | 8 | | Sy 1.5 | | 10.40 | 0.342 | |
| 16..... | SWIFT J0234.6-0848 | NGC 985 | 38.6574 | -8.7876 | y* | 5.07 | 3.7 | 0.043 | 44.21 | 21.59 | 8 | y | Sy 1† | | 11.63 | 1.281 | |
| 17..... | SWIFT J0235.3-2934 | ESO 416-G002 | 38.8058 | -29.6047 | y | 4.76 | 3.2 | 0.059198 | 44.42 | <19.60 | 9 | | Sy 1.9 | | 12.15 | 0.356 | |
| 18..... | SWIFT J0238.2-5213 ¹ | ESO 198-024 | 39.5821 | -52.1923 | y* | 7.82 | 3.9 | 0.0455 | 44.27 | 21.00 | 8 | | Sy 1 | | 12.68 | 2.380 | |
| 19..... | SWIFT J0244.8+6227 | QSO B0241+622 | 41.2404 | 62.4685 | | 11.19 | 7.3 | 0.044 | 44.52 | 21.98 | 10 | | Sy 1 | | | 0.414 | |
| 20..... | SWIFT J0255.2-0011 ¹ | NGC 1142 | 43.8008 | -0.1836 | y* | 9.80 | 7.8 | 0.028847 | 44.17 | 23.38 | 9 | y | Sy 2† | | 10.06 | 0.011 | |
| 21..... | SWIFT J0318.7+6828 | 2MASX J03181899+6829322 | 49.5791 | 68.4921 | | 4.89 | 3.5 | 0.0901 | 44.85 | 22.59 | 1 | | Sy 1.9 | 36 | 15.13 | | |
| 22..... | SWIFT J0319.7+4132 | NGC 1275 | 49.9507 | 41.5117 | | 13.51 | 11.5 | 0.017559 | 43.90 | 21.18 | 11 | | Sy 2 | | 11.02 | 4.756 | |
| 23..... | SWIFT J0328.4-2846 | PKS 0326-288 | 52.1521 | -28.6968 | y | 4.50 | 2.3 | 0.108 | 44.84 | | | | Sy 1.9 | 37 | 14.19 | | |
| 24..... | SWIFT J0333.6-3607 ¹ | NGC 1365 | 53.4015 | -36.1404 | y* | 13.93 | 7.2 | 0.005457 | 42.67 | 23.60 | 4 | y | Sy 1.8 | | 7.36 | 0.101 | |
| 25..... | SWIFT J0342.0-2115 | ESO 548-G081 | 55.5155 | -21.2444 | y* | 5.45 | 3.3 | 0.01448 | 43.19 | 20.48 | 1 | | Sy 1 | | 9.35 | 0.258 | |
| 26..... | SWIFT J0349.2-1159 | IES 0347-121 | 57.3467 | -11.9908 | y* | 5.29 | 3.6 | 0.18 | 45.51 | 20.55 | 8 | | BL Lac | | | 1.210 | |
| 27..... | SWIFT J0350.1-5019 | PGC 13946 | 57.5990 | -50.3099 | y* | 5.99 | 2.9 | 0.036492 | 43.95 | 22.72 | 1 | | Galaxy | 35 | 11.68 | | |
| 28..... | SWIFT J0356.9-4041 | 2MASX J03565655-4041453 | 59.2356 | -40.6960 | y* | 5.22 | 2.4 | 0.0747 | 44.51 | 22.52 | 1 | | Sy 1.9 | 37 | 13.27 | 0.007 | |
| 29..... | SWIFT J0407.4+0339 | 3C 105 | 61.8186 | 3.7071 | y | 4.01 | 3.4 | 0.089 | 44.83 | 23.43 | 1 | | Sy 2 | | 15.16 | 0.398 | |
| 30..... | SWIFT J0418.3+3800 | 3C 111.0 | 64.5887 | 38.0266 | | 13.41 | 12.5 | 0.0485 | 44.84 | 21.98 | 8 | | Sy 1 | | 13.63 | 4.563 | |
| 31..... | SWIFT J0426.2-5711 | IH 0419-577 | 66.5035 | -57.2001 | y* | 5.49 | 2.9 | 0.104 | 44.91 | 19.52 | 8 | | Sy 1 | | | 2.174 | |
| 32..... | SWIFT J0433.0+0521 ¹ | 3C 120 | 68.2962 | 5.3543 | y* | 13.15 | 11.2 | 0.03301 | 44.45 | 21.19 | 8 | | Sy 1 | | 11.69 | | |
| 33..... | SWIFT J0444.1+2813 | 2MASX J04440903+2813003 | 71.0376 | 28.2168 | | 7.15 | 7.6 | 0.01127 | 43.33 | 22.72 | 1 | | Sy 2 | | 10.88 | 0.281 | |
| 34..... | SWIFT J0451.4-0346 ¹ | MCG -01-13-025 | 72.9230 | -3.8094 | y* | 5.62 | 4.5 | 0.015894 | 43.41 | 20.62 | 7 | | Sy 1.2 | | 11.14 | 0.590 | |
| 35..... | SWIFT J0452.2+4933 | IRXS J045205.0+493248 | 73.0208 | 49.5459 | | 7.59 | 5.6 | 0.029 | 44.04 | 21.65 | 1 | | Sy 1 | | 12.26 | 0.009 | |
| 36..... | SWIFT J0505.8-2351 | XSS J05054-2348 | 76.4405 | -23.8539 | y* | 11.26 | 6.1 | 0.035043 | 44.24 | 22.69 | 1 | | Sy 2 | | 13.77 | 0.670 | |
| 37..... | SWIFT J0510.7+1629 | 4U 0517+17 | 77.6896 | 16.4988 | | 7.12 | 7.8 | 0.017879 | 43.75 | | | | Sy 1.5 | | | 0.210 | |
| 38..... | SWIFT J0516.2-0009 ¹ | Ark 120 | 79.0476 | -0.1498 | y* | 7.12 | 5.3 | 0.032296 | 44.11 | 20.30 | 4 | | Sy 1 | | 11.26 | 2.120 | |
| 39..... | SWIFT J0501.9-3239 | ESO 362-G018 | 79.8992 | -32.6578 | y* | 10.49 | 5.1 | 0.012642 | 43.26 | 20.25 | | y | Sy 1.5 | | 11.10 | 0.060 | |
| 40..... | SWIFT J0519.5-4545 | PICTOR A | 79.9570 | -45.7790 | y | 4.23 | 2.2 | 0.035058 | 43.80 | 21.00 | 8 | | Sy 1/Liner | | 13.63 | 0.626 | |
| 41..... | SWIFT J0519.5-3140 | PKS 0521-365 | 80.7416 | -36.4586 | y* | 6.02 | 2.8 | 0.05534 | 44.31 | 21.11 | 8 | | BL Lac | | 12.50 | 0.883 | |
| 42..... | SWIFT J0538.8-4405 | PKS 0537-441 | 84.7098 | -44.0858 | y* | 5.79 | 3.1 | 0.8904 | 47.09 | 20.54 | 12 | | BL Lac | | 13.45 | 0.178 | |
| 43..... | SWIFT J0539.9-2839 | [HB89] 0537-286 | 84.9762 | -28.6655 | y | 4.27 | 2.5 | 3.104 | 48.32 | 20.77 | 8 | | Blazar | | 13.59 | 0.092 | |
| 44..... | SWIFT J0550.7-3212 | PKS 0548-322 | 87.6699 | -32.2716 | y* | 7.39 | 4.4 | 0.069 | 44.70 | 21.50 | 8 | | BL Lac | | | 2.533 | |
| 45..... | SWIFT J0552.2-0727 | NGC 2110 | 88.0474 | -7.4562 | y* | 32.46 | 25.6 | 0.007789 | 43.54 | 22.57 | 8 | | Sy 2 | | 9.26 | 0.010 | |
| 46..... | SWIFT J0554.8+4625 | MCG +08-11-011 | 88.7234 | 46.4393 | | 11.37 | 11.1 | 0.020484 | 44.02 | 20.30 | 4 | | Sy 1.5 | | 10.49 | 1.689 | |
| 47..... | SWIFT J0557.9-3822 ¹ | EXO 055620-3820.2 | 89.5083 | -38.3346 | y* | 9.82 | 5.2 | 0.03387 | 44.14 | 22.23 | 8 | | Sy 1 | | 11.86 | 0.105 | |

TABLE 1—Continued

| No. | Swift Name ^a | ID ^b | R.A. ^c (deg) | Decl. ^c (deg) | >15 ^{c,d} | SNR | f_{BAT}^e | z | $\log L^e$ (erg s ⁻¹) | $\log \eta_{\text{H}}^e$ (cm ⁻²) | Ref. ^f | Complex ^g | Type ^b | Note ⁱ | J (mag) | $f_{\text{ROSAT}}^{\text{Rate},k}$ |
|-----|---------------------------------|--------------------------|----------------------------|-----------------------------|--------------------|-------|--------------------|----------|--------------------------------------|---|-------------------|----------------------|-------------------|-------------------|--------------|------------------------------------|
| 48 | SWIFT J0602.2+2829 | IRAS 05589+2828 | 90.5446 | 28.4728 | | 5.08 | 5.6 | 0.033 | 44.15 | 21.57 | 1 | | Sy 1 | | | 0.866 |
| 49 | SWIFT J0601.9−8636 | ESO 005−G004 | 91.4235 | −86.6319 | y* | 5.64 | 4.2 | 0.006228 | 42.56 | 23.88 | 1 | | Sy 2† | 38 | 9.53 | 0.061 |
| 50 | SWIFT J0615.8+7101 ¹ | Mrk 3 | 93.9015 | 71.0375 | y* | 14.27 | 10.1 | 0.013509 | 43.61 | 24.00 | 13 | y | Sy 2 | | 10.03 | 0.011 |
| 51 | SWIFT J0623.9−6058 | ESO 121−IG 028 | 95.9399 | −60.9790 | y* | 4.85 | 2.8 | 0.0403 | 44.03 | 23.20 | | | Sy 2 | 39 | 11.63 | 0.273 |
| 52 | SWIFT J0640.4−2554 | ESO 490−IG 026 | 100.0487 | −25.8954 | | 5.14 | 3.6 | 0.0248 | 43.71 | 21.48 | 1 | | Sy 1.2 | | 11.09 | |
| 53 | SWIFT J0640.1−4328 | 2MASX J06403799−4321211 | 100.1583 | −43.3558 | y | 4.51 | 2.8 | | 23.04 | 23.04 | 1 | | Galaxy† | 35 | 14.24 | |
| 54 | SWIFT J0641.3+3257 | 2MASX J06411806+3249313 | 100.3252 | 32.8254 | | 5.51 | 5.5 | 0.047 | 44.46 | 22.98 | 9 | | Sy 2 | 40 | 14.01 | 0.062 |
| 55 | SWIFT J0742.5+4948 | Mrk 6 | 103.0510 | 74.4271 | y* | 9.55 | 6.6 | 0.01881 | 43.72 | 23.00 | 14 | y | Sy 1.5 | | 11.07 | 2.196 |
| 56 | SWIFT J0742.5+4948 | Mrk 79 | 115.6367 | 49.8097 | y* | 7.09 | 4.7 | 0.022189 | 43.72 | 20.76 | 15 | | Sy 1.2 | | 11.19 | 0.032 |
| 57 | SWIFT J0746.3+2548 | SDSS J074625.87+254902.2 | 116.6078 | 25.8173 | y* | 5.92 | 4.7 | 2.9793 | 48.55 | 22.00 | 16 | | Blazar | 16 | | 0.755 |
| 58 | SWIFT J0759.8−3844 | IGR J07597−3842 | 119.9208 | −38.7600 | | 7.79 | 5.3 | 0.04 | 44.29 | 21.70 | 1 | | Sy 1.2 | | | |
| 59 | SWIFT J0841.4+7052 ¹ | [HB89] 0836+710 | 130.3515 | 70.8951 | y* | 11.38 | 7.0 | 2.172 | 48.39 | 20.98 | 8 | | Blazar | 41 | 11.50 | |
| 60 | SWIFT J0902.0+6007 | Mrk 18 | 135.4933 | 60.1517 | y* | 5.35 | 3.1 | 0.011088 | 42.93 | 23.39 | 9 | | Galaxy | | | |
| 61 | SWIFT J0904.3+5538 | 2MASX J09043699+5536025 | 136.1539 | 55.6007 | y* | 5.21 | 3.4 | 0.037 | 44.03 | 21.89 | 1 | | Sy 1 | | 13.55 | |
| 62 | SWIFT J0911.2+4533 | 2MASX J09112999+4528060 | 137.8749 | 45.4683 | y* | 5.35 | 3.0 | 0.026782 | 43.69 | 23.42 | 1 | | Sy 2 | | 13.18 | |
| 63 | SWIFT J0917.2−6221 | IRAS 091749−6206 | 139.0371 | −62.3249 | | 4.51 | 3.2 | 0.0573 | 44.40 | 22.19 | 1 | | Sy 1 | 42 | 14.91 | 0.120 |
| 64 | SWIFT J0918.5+0425 | 2MASX J09180027+0425066 | 139.5011 | 4.4184 | y | 4.72 | 3.1 | 0.156 | 45.31 | 23.00 | 1 | | QSO 2** | | | |
| 65 | SWIFT J0920.8−0805 | MCG −01−24−012 | 140.1927 | −8.0561 | y* | 6.44 | 4.6 | 0.019644 | 43.60 | 22.80 | 12 | | Sy 2 | | 13.18 | 1.626 |
| 66 | SWIFT J0923.7+2255 ¹ | MCG +04−22−042 | 140.9292 | 22.9090 | y* | 6.38 | 4.1 | 0.032349 | 43.99 | 20.60 | 1 | | Sy 1.2 | | 11.83 | 1.691 |
| 67 | SWIFT J0925.0+5218 ¹ | Mrk 110 | 141.3036 | 52.2863 | y* | 9.26 | 5.4 | 0.03529 | 44.19 | 20.58 | 8 | | Sy 1 | | 13.20 | 0.280 |
| 68 | SWIFT J0945.6−1420 ¹ | NGC 2992 | 146.4252 | −14.3264 | y* | 9.07 | 6.6 | 0.007709 | 42.94 | 22.47 | 17 | | Sy 2 | | 9.67 | 0.256 |
| 69 | SWIFT J0947.6−3057 | MCG −05−23−016 | 146.9173 | −30.9489 | y* | 28.67 | 21.9 | 0.008486 | 43.55 | 22.47 | 18 | | Sy 2 | | 10.53 | 0.008 |
| 70 | SWIFT J0959.5−2248 ¹ | NGC 3081 | 149.8731 | −22.8263 | y* | 11.34 | 8.8 | 0.007956 | 43.09 | 23.52 | 19 | | Sy 2 | | 9.91 | 0.100 |
| 71 | SWIFT J1023.5+1952 ¹ | NGC 3227 | 155.8775 | 19.8650 | y* | 22.01 | 12.9 | 0.003859 | 42.63 | 22.80 | 20 | | Sy 1.5 | | 8.59 | 0.012 |
| 72 | SWIFT J1031.7−3451 ¹ | NGC 3281 | 157.9670 | −34.8537 | y* | 10.24 | 7.3 | 0.010674 | 43.27 | 24.30 | 12 | | Sy 2 | 43 | 13.24 | 0.100 |
| 73 | SWIFT J1038.8−4942 | 2MASX J10384520−4946531 | 159.6854 | −49.7826 | | 4.86 | 3.3 | 0.06 | 44.46 | 22.17 | 1 | | Sy 1† | | 11.44 | 0.007 |
| 74 | SWIFT J1040.7−4619 | LEDA 093974 | 160.0939 | −46.4238 | | 4.26 | 3.4 | 0.023923 | 43.64 | 22.96 | 1 | | Sy 2 | | 12.74 | |
| 75 | SWIFT J1049.4+2258 | Mrk 417 | 162.3789 | 22.9644 | y* | 6.39 | 3.6 | 0.032756 | 43.95 | 23.60 | 9 | | Sy 2 | | 11.09 | 16.220 |
| 76 | SWIFT J1104.4+3812 ¹ | Mrk 421 | 166.1138 | 38.2088 | y* | 14.02 | 6.8 | 0.030021 | 44.15 | 20.30 | 21 | | BL Lac | | 9.74 | 4.280 |
| 77 | SWIFT J1106.5+7234 ¹ | NGC 3516 | 166.6979 | 72.5686 | y* | 18.26 | 10.6 | 0.008836 | 43.26 | 21.21 | 8 | | Sy 1.5 | 33 | | |
| 78 | SWIFT J1127.5+1906 | RX J1127.2+1909 | 171.8178 | 19.1556 | y | 4.14 | 2.2 | 0.1055 | 44.79 | 21.30 | 1 | | Sy 1.8 | | | |
| 79 | SWIFT J1139.0−3743 ¹ | NGC 3783 | 174.7572 | −37.7386 | y* | 20.46 | 16.1 | 0.00973 | 43.53 | 22.47 | 4 | | Sy 1 | | 9.83 | 1.130 |
| 80 | SWIFT J1139.1+5913 | SBS 1136+594 | 174.7873 | 59.1985 | y | 4.64 | 2.5 | 0.0601 | 44.33 | 19.58 | 1 | | Sy 1.5 | | 14.83 | 0.372 |
| 81 | SWIFT J1143.7+7942 | UGC 06728 | 176.3168 | 79.6815 | y* | 5.88 | 3.7 | 0.006518 | 42.54 | 20.65 | 9 | | Sy 1.2 | | 11.62 | 0.375 |
| 82 | SWIFT J1145.6−1819 | 2MASX J11454045−1827149 | 176.4186 | −18.4543 | y* | 5.26 | 3.9 | 0.032949 | 43.98 | 20.54 | 1 | | Sy 1 | | 13.93 | 3.293 |
| 83 | SWIFT J1200.8+0650 | CGCG 041−020 | 180.2413 | 6.8064 | y | 4.53 | 2.5 | 0.036045 | 43.88 | 22.83 | 1 | | Sy 2 | 42 | 12.15 | |
| 84 | SWIFT J1200.2−5350 | IGR J12026−5349 | 180.6985 | −53.8355 | | 5.37 | 4.0 | 0.027966 | 43.86 | 22.34 | | | Sy 2 | | | 0.026 |
| 85 | SWIFT J1203.0+4433 | NGC 4051 | 180.7900 | 44.5313 | y* | 9.01 | 4.6 | 0.002335 | 41.74 | 20.47 | 8 | | Sy 1.5 | | 11.48 | 3.918 |
| 86 | SWIFT J1204.5+2019 | Ark 347 | 181.1237 | 20.3162 | y | 4.39 | 2.3 | 0.02244 | 43.42 | 23.20 | 1 | | Sy 2 | | 11.76 | 0.004 |
| 87 | SWIFT J1206.2+5243 | NGC 4102 | 181.5963 | 52.7109 | y* | 5.00 | 2.4 | 0.002823 | 41.62 | 20.94 | 22 | | Linear | | 8.76 | |
| 88 | SWIFT J1209.4+4340 ¹ | NGC 4138 | 182.3741 | 43.6853 | y | 4.53 | 2.1 | 0.002962 | 41.62 | 22.90 | 23 | | Sy 1.9 | | 9.90 | |
| 89 | SWIFT J1210.5+3924 ¹ | NGC 4151 | 182.6358 | 39.4057 | y* | 74.10 | 37.4 | 0.003319 | 42.96 | 22.48 | 24 | | Sy 1.5 | | 8.50 | 0.651 |
| 90 | SWIFT J1218.5+2952 | Mrk 766 | 184.6105 | 29.8129 | y | 4.60 | 2.3 | 0.012929 | 42.94 | 21.72 | 8 | | Sy 1.5 | | 11.10 | 4.710 |
| 91 | SWIFT J1225.8+1240 ¹ | NGC 4388 | 186.4448 | 12.6621 | y* | 45.63 | 25.3 | 0.008419 | 43.60 | 23.63 | 4 | | Sy 2 | | 8.98 | 0.516 |
| 92 | SWIFT J1202.5+3332 | NGC 4395 | 186.4538 | 33.5468 | y* | 5.05 | 2.6 | 0.001064 | 40.81 | 22.30 | | | Sy 1.9 | | 10.66 | |
| 93 | SWIFT J1229.1+0202 ¹ | 3C 273 | 187.2779 | 2.0524 | y* | 44.58 | 26.2 | 0.15834 | 46.25 | 20.54 | 8 | | Blazar | | 11.69 | 7.905 |
| 94 | SWIFT J1235.6−3954 ¹ | NGC 4507 | 188.9026 | −39.9093 | y* | 23.56 | 19.3 | 0.011802 | 43.78 | 23.46 | 4 | | Sy 2 | | 9.93 | 0.032 |
| 95 | SWIFT J1238.9−2720 | ESO 506−G027 | 189.7275 | −27.3078 | y* | 16.87 | 13.2 | 0.025024 | 44.28 | 23.60 | 1 | | Sy 2 | 43 | 11.14 | |

TABLE 1—Continued

| No. | Swift Name ^a | ID ^b | R.A. ^c (deg) | Decl. ^c (deg) | >15 ^{cd} | SNR | f_{BAT}^e | z | $\log L^e$ (erg s ⁻¹) | $\log \eta_{\text{H}}$ (cm ⁻²) | Ref. ^f | Complex ^g | Type ^h | Note ⁱ | J (mag) | $f_{\text{ROSAT}} \text{ Rate}^{\text{jk}}$ |
|----------|---------------------------------|-------------------------|----------------------------|-----------------------------|-------------------|-------|--------------------|----------|--------------------------------------|---|-------------------|----------------------|-------------------|-------------------|--------------|---|
| 96..... | SWIFT J1239.3-1611 | XSS J12389-1614 | 189.7763 | -16.1799 | y* | 8.57 | 5.8 | 0.036675 | 44.26 | 22.48 | 1 | | Sy 2 | 44 | 11.48 | |
| 97..... | SWIFT J1239.6-0519 ^l | NGC 4593 | 189.9142 | -5.3442 | y* | 14.62 | 9.1 | 0.009 | 43.21 | 20.30 | 4 | y | Sy 1 [†] | | 8.96 | 1.429 |
| 98..... | SWIFT J1241.6-5748 | WKK 1263 | 190.3572 | -57.8343 | | 4.09 | 2.8 | 0.02443 | 43.58 | 21.50 | 9 | | Sy 2 [†] | | 12.29 | 0.614 |
| 99..... | SWIFT J1256.2-0551 | 3C 279 | 194.0465 | -5.7893 | y* | 5.47 | 3.2 | 0.5362 | 46.57 | 20.41 | 8 | | Blazar | | 19.90 | 0.400 |
| 100..... | SWIFT J1303.8+5345 | SBS 1301+540 | 195.9978 | 53.7917 | y* | 4.82 | 2.5 | 0.02988 | 43.72 | 20.60 | 1 | | Sy 1 | 45 | 13.43 | 0.059 |
| 101..... | SWIFT J1305.4-4928 | NGC 4945 | 196.3645 | -49.4682 | | 24.48 | 19.4 | 0.001878 | 42.18 | 24.60 | 4 | | Sy 2 [†] | | 5.60 | 0.085 |
| 102..... | SWIFT J1309.2+1139 | NGC 4992 | 197.3040 | 11.6459 | y* | 8.45 | 4.7 | 0.025137 | 43.83 | 23.39 | 9 | y | Galaxy | 46 | 11.23 | |
| 103..... | SWIFT J1322.2-1641 ^l | MCG -03-34-064 | 200.6019 | -16.7286 | y* | 6.53 | 4.7 | 0.016541 | 43.46 | 23.59 | 23 | | Sy 1.8 | | 10.80 | 0.411 |
| 104..... | SWIFT J1325.4-4301 ^l | Cen A | 201.3650 | -43.0192 | y* | 93.44 | 74.8 | 0.001825 | 42.74 | 22.74 | 8 | | Sy 2 | | 4.98 | |
| 105..... | SWIFT J1335.8-3416 | MCG -06-30-015 | 203.9741 | -34.2956 | y* | 9.26 | 7.5 | 0.007749 | 43.00 | 21.67 | 8 | | Sy 1.2 | | 10.87 | 2.496 |
| 106..... | SWIFT J1338.2+0433 | NGC 5252 | 204.5665 | 4.5426 | y* | 10.52 | 6.6 | 0.022975 | 43.90 | 25.82 | 8 | y | Sy 1.9 | | 10.89 | |
| 107..... | SWIFT J1347.4-6033 | 4U 1344-60 | 206.8500 | -60.6400 | | 8.93 | 7.0 | 0.012879 | 45.49 | 22.37 | 6 | | Sy 1.5 | | | 2.960 |
| 108..... | SWIFT J1349.3-3018 ^l | IC 4329A | 207.3304 | -30.3096 | y* | 33.62 | 30.0 | 0.016054 | 44.24 | 21.65 | 8 | | Sy 1.2 | | 10.24 | |
| 109..... | SWIFT J1352.8+6917 ^l | Mrk 279 | 208.2644 | 69.3082 | y* | 8.67 | 4.4 | 0.030451 | 43.97 | 20.53 | 8 | | Sy 1.5 | | 11.43 | 2.809 |
| 110..... | SWIFT J1413.2-0312 ^l | NGC 5506 | 213.3119 | -3.2075 | y* | 30.36 | 23.6 | 0.006181 | 43.30 | 22.53 | 4 | | Sy 1.9 | | 9.71 | 0.110 |
| 111..... | SWIFT J1417.7+2539 | 1E 1415+259 | 214.4862 | 25.7240 | y* | 4.92 | 3.1 | 0.237 | 45.71 | 20.72 | 1 | | BL Lac | 47 | 1.710 | 1.710 |
| 112..... | SWIFT J1417.9+2507 | NGC 5548 | 214.4981 | 25.1368 | y* | 5.73 | 4.7 | 0.022339 | 43.73 | 21.21 | 8 | y | Sy 1.5 | | 10.64 | 4.950 |
| 113..... | SWIFT J1419.0-2639 | ESO 511-G030 | 214.8434 | -26.6447 | y* | 9.11 | 5.8 | 0.01717 | 43.59 | 20.41 | 8 | | Sy 1 | | 10.79 | 1.221 |
| 114..... | SWIFT J1428.7+4234 | 1ES 1426+428 | 217.1361 | 42.6724 | y | 4.66 | 2.6 | 0.129 | 45.06 | 21.52 | 8 | | Sy 1 | | 13.04 | 0.885 |
| 115..... | SWIFT J1442.5-1715 ^l | NGC 5728 | 220.5997 | -17.2532 | y* | 8.96 | 8.9 | 0.0093 | 43.23 | 23.63 | 25 | | Sy 2 | | 9.18 | |
| 116..... | SWIFT J1504.2+1025 | Mrk 841 | 226.0050 | 10.4378 | y* | 5.56 | 5.1 | 0.036422 | 44.20 | 21.32 | 8 | y | Sy 1 | | 12.56 | 0.081 |
| 117..... | SWIFT J1535.9+5751 | Mrk 290 | 233.9682 | 57.9026 | y* | 4.66 | 3.0 | 0.029577 | 43.79 | 20.40 | 8 | | Sy 1 | | 13.04 | 0.885 |
| 118..... | SWIFT J1628.1+5145 ^l | Mrk 1498 | 247.0169 | 51.7754 | y* | 6.13 | 4.5 | 0.0547 | 44.50 | 23.26 | 1 | | Sy 1.9 | | 12.77 | |
| 119..... | SWIFT J1648.0-3037 | 2MASX J16481523-3035037 | 252.0635 | -30.5845 | | 6.38 | 8.6 | 0.031 | 44.28 | 21.61 | 1 | | Sy 1 | | 12.56 | 0.149 |
| 120..... | SWIFT J1652.9+0223 | NGC 6240 | 253.2454 | 2.4008 | y | 4.43 | 4.7 | 0.02448 | 43.81 | 24.34 | 4 | | Sy 2 | | 10.30 | 0.090 |
| 121..... | SWIFT J1654.0+3946 | Mrk 501 | 253.4676 | 39.7602 | y* | 7.63 | 4.9 | 0.03366 | 44.11 | 22.40 | 8 | y | BL Lac | | 10.67 | 4.122 |
| 122..... | SWIFT J1717.1-6249 | NGC 6300 | 259.2478 | -62.8206 | | 8.76 | 9.1 | 0.003699 | 42.44 | 23.34 | 1 | | Sy 2 | | 7.86 | |
| 123..... | SWIFT J1737.5-2908 | GRS 1734-292 | 264.3512 | -29.1800 | | 8.63 | 10.9 | 0.0214 | 44.05 | 20.67 | 26 | | Sy 1 | | | |
| 124..... | SWIFT J1745.4+2906 | IRXS J174538.1+290823 | 266.4094 | 29.1395 | y* | 5.62 | 3.9 | 0.011332 | 44.81 | 21.13 | 1 | | Sy 1 | 40 | 13.98 | 0.530 |
| 125..... | SWIFT J1835.0+3240 | 3C 382 | 278.7590 | 32.6973 | y* | 10.96 | 8.1 | 0.05787 | 44.81 | 21.13 | 8 | | Sy 1 | | 11.87 | 2.000 |
| 126..... | SWIFT J1838.4-6524 ^l | ESO 103-035 | 279.5847 | -65.4276 | y* | 9.50 | 9.7 | 0.013286 | 43.58 | 23.17 | 8 | | Sy 2 | | 11.38 | 0.060 |
| 127..... | SWIFT J1842.0+7945 ^l | 3C 390.3 | 280.5375 | 79.7714 | y* | 17.32 | 10.1 | 0.0561 | 44.88 | 21.03 | 8 | | Sy 1 | | 12.91 | 0.472 |
| 128..... | SWIFT J1930.5+3414 | NVSS J193013+341047 | 292.5554 | 34.1797 | | 5.92 | 3.3 | 0.0629 | 44.50 | 23.20 | 27 | | Sy 1 | 48 | 14.24 | |
| 129..... | SWIFT J1942.6-1024 | NGC 6814 | 295.6694 | -10.3235 | y* | 5.68 | 6.2 | 0.005214 | 42.57 | 20.76 | 28 | | Sy 1.5 | | 8.66 | 0.034 |
| 130..... | SWIFT J1952.4+0237 | 3C 403 | 298.0658 | 2.5068 | | 4.29 | 4.1 | 0.059 | 44.53 | 23.60 | 22 | | Sy 2 | | 12.53 | 0.947 |
| 131..... | SWIFT J1959.4+4044 | Cyg A | 299.8681 | 40.7339 | | 16.74 | 10.9 | 0.05607 | 44.91 | 23.30 | 29 | | Sy 2 | | 10.61 | 2.653 |
| 132..... | SWIFT J1959.6+6507 | IES 1959+650 | 299.9994 | 65.1485 | y* | 6.68 | 4.1 | 0.047 | 44.33 | 21.11 | 15 | | BL Lac | | 12.54 | 0.566 |
| 133..... | SWIFT J2009.0-6103 | NGC 6860 | 302.1954 | -61.1002 | y* | 5.08 | 4.9 | 0.014884 | 43.39 | 21.75 | 1 | y | Sy 1 | | 10.68 | |
| 134..... | SWIFT J2028.5+2543a | MCG +04-48-002 | 307.1463 | 25.7336 | | 9.05 | 6.1 | 0.0139 | 43.42 | 23.60 | 1 | | Sy 2 | | 11.23 | |
| 135..... | SWIFT J2028.5+2543b | NGC 6921 | 307.1203 | 25.7234 | | 9.05 | 6.1 | 0.014467 | 43.45 | 23.96 | 3 | y | Sy 2 | | 10.01 | |
| 136..... | SWIFT J2042.3+7507 ^l | 4C +74.26 | 310.6554 | 75.1340 | y* | 8.52 | 5.0 | 0.104 | 45.14 | 21.25 | 30 | y | Sy 1 | 49 | 11.58 | 0.588 |
| 137..... | SWIFT J2044.2-1045 ^l | Mrk 509 | 311.0406 | -10.7235 | y* | 8.36 | 9.7 | 0.0344 | 44.43 | 20.70 | 8 | | Sy 1.2 | | 11.10 | 3.850 |
| 138..... | SWIFT J2052.0-5704 ^l | IC 5063 | 313.0097 | -57.0688 | y* | 7.90 | 7.1 | 0.011348 | 43.31 | 23.28 | 8 | y | Sy 2 | | 13.17 | 0.010 |
| 139..... | SWIFT J2114.4+8206 | 2MASX J21140128+8204483 | 318.5049 | 82.0801 | y* | 5.86 | 3.6 | 0.084 | 44.80 | 21.11 | 1 | | Sy 1 [†] | | 10.60 | 0.460 |
| 140..... | SWIFT J2124.6+5057 | IGR J21247+5058 | 321.1589 | 50.9828 | | 21.74 | 13.9 | 0.02 | 44.10 | 22.39 | 1 | | Sy 1 | 50 | 0.026 | |
| 141..... | SWIFT J2127.4+5654 | IGR J21277+5656 | 321.9413 | 56.9429 | | 4.21 | 2.7 | 0.0147 | 43.12 | 21.98 | 1 | | Sy 1 | 44 | 0.310 | |
| 142..... | SWIFT J2156.1+4728 | RX J2135.9+4728 | 323.9792 | 47.4731 | | 4.48 | 2.9 | 0.025 | 43.61 | 21.78 | 1 | | Sy 1 | | 12.79 | 0.124 |
| 143..... | SWIFT J2152.0-3030 | PKS 2149-306 | 327.9812 | -30.4650 | y* | 5.08 | 5.4 | 2.345 | 48.36 | 20.52 | 1 | | Blazar | | | 0.462 |

TABLE 1—Continued

| No. | Swift Name ^a | ID ^b | R.A. ^c (deg) | Decl. ^c (deg) | >15 ^σ ^d | SNR | $f_{\text{BAT}}^{\text{e}}$ | z | $\log L^{\text{e}}$ (erg s ⁻¹) | $\log n_{\text{H}}$ (cm ⁻²) | Ref. ^f | Complex ^g | Type ^h | Note ⁱ | J (mag) | f_{ROSAT} | Rate ^{j,k} |
|----------|---------------------------------|-----------------|----------------------------|-----------------------------|-------------------------------|-------|-----------------------------|----------|---|--|-------------------|----------------------|-------------------|-------------------|--------------|--------------------|---------------------|
| 144..... | SWIFT J2200.9+1032 | UGC 11871 | 330.1724 | 10.5524 | y | 4.52 | 3.9 | 0.026612 | 43.80 | 22.21 | 1 | | Sy 1.9 | | 11.72 | | |
| 145..... | SWIFT J2201.9-3152 ^l | NGC 7172 | 330.5080 | -31.8698 | y* | 12.28 | 12.4 | 0.008683 | 43.32 | 22.89 | 8 | | Sy 2 | | 9.44 | | 0.012 |
| 146..... | SWIFT J2209.4-4711 | NGC 7213 | 332.3177 | -47.1667 | y* | 6.70 | 5.2 | 0.005839 | 42.59 | 20.60 | 8 | y | Sy 1.5 | | 7.97 | | 3.940 |
| 147..... | SWIFT J2235.9-2602 | NGC 7314 | 338.9426 | -26.0502 | y* | 5.24 | 5.7 | 0.00476 | 42.45 | 21.79 | 8 | y | Sy 1.9† | | 9.06 | | 0.236 |
| 148..... | SWIFT J2235.9+3358 | NGC 7319 | 339.0148 | 33.9757 | y* | 6.23 | 4.1 | 0.022507 | 43.68 | 23.38 | 25 | y | Sy 2 | | 11.09 | | 0.001 |
| 149..... | SWIFT J2246.0+3941 | 3C 452 | 341.4532 | 39.6877 | y | 4.78 | 3.3 | 0.0811 | 44.73 | 23.43 | 31 | | Sy 2 | | 13.35 | | |
| 150..... | SWIFT J2253.9+1608 | 3C 454.3 | 343.4906 | 16.1482 | y* | 21.25 | 19.0 | 0.859 | 47.83 | 20.77 | 32 | | Blazar | | 14.50 | | 0.263 |
| 151..... | SWIFT J2254.1-1734 ^l | MR 2251-178 | 343.5242 | -17.5819 | y* | 9.53 | 10.8 | 0.06398 | 45.03 | 20.80 | 8 | y | Sy 1 | | 12.54 | | 1.037 |
| 152..... | SWIFT J2303.3+0852 | NGC 7469 | 345.8151 | 8.8740 | y* | 9.35 | 8.3 | 0.016317 | 43.70 | 20.61 | 8 | | Sy 1.2 | | 10.11 | | 1.700 |
| 153..... | SWIFT J2304.8-0843 | Mrk 926 | 346.1811 | -8.6857 | y* | 5.19 | 5.5 | 0.04686 | 44.45 | 21.14 | 8 | | Sy 1.5 | | 11.84 | | 3.530 |
| 154..... | SWIFT J2318.4-4223 ^l | NGC 7582 | 349.5979 | -42.3706 | y* | 10.24 | 6.7 | 0.005254 | 42.61 | 22.98 | 8 | y | Sy 2 | | 8.35 | | 0.048 |

NOTE.—Double asterisk (**), indicates that we classify 2MASX J09180027+0425066 as a QSO because its luminosity is greater than $10^{44.5}$ erg cm⁻² s⁻¹, and as type II because of its very strong narrow O III lines in SSDS.

^a The Swift name given is based on the source coordinates from the latest analysis of Swift data except that where a name has been previously published it is kept to avoid confusion.

^b The ID name given is that of the entry in the NED database (except in those few cases there is none).

^c J2000.0 coordinates for the identified counterpart.

^d A “y” indicates that the source is at $|b| > 15^\circ$ and so, if the SNR is also $> 4.8\sigma$ (indicated by “y*”), is included in the quantitative analysis.

^e BAT fluxes (in units of 10^{-11} erg cm⁻² s⁻¹) and luminosities are in the band 14–195 keV. Distances for luminosity were calculated using the measured redshift and assuming it was due to Hubble flow. Luminosity errors must include the error in measured flux and the error in distance due to the random velocity of galaxies (~ 500 km s⁻¹).

^f Reference for the n_{H} value; see below.

^g “Complex = y” indicates that the spectrum differs significantly from a simple power law with absorption and an Fe line.

^h This column contains optically derived types. For well-studied AGNs, the optical type was derived from Véron-Cetty & Véron (2006). For the remaining sources, we determined type by examining the spectrum from archival data or from our own observations. The few remaining AGNs without an accessible spectrum are flagged with a dagger (†).

ⁱ Reference for the type and/or z , where this is not from NED; see below.

^j ROSAT flux in counts s⁻¹ from the HEASARC database (Schwope et al. 2000).

^k The J band is better to use than the K band because it is expected to have a better sensitivity in detecting local AGNs. The colors of hard X-ray selected AGNs have J/K values ~ 1 at low redshifts, and galaxies at low z also have $J/K \sim 1$ (Watanabe et al. 2004). The 2MASS survey is more sensitive in J (see [http://www.ipac.caltech.edu/2mass/releases/second/doc/figures/secvi2af5.grf](http://www.ipac.caltech.edu/2mass/releases/second/doc/figures/second/doc/figures/secvi2af5.grf), where it is shown that the survey goes ~ 1 mag more sensitive in J than K).

^l Sources detected in the 3 month survey (Markwardt et al. 2005).

REFERENCES.— Double daggers (††) indicate our interpretation of published spectra. (1) Swift XRT; (2) XTE/Akylas et al. 2002; (3) XMM/L. M. Winter et al. 2008a, in preparation; (4) Lutz et al. 2004; (5) Sambruna et al. 1998; (6) ASCA/R. F. Mushotzky et al. 2008, in preparation; (7) Gallo et al. 2006; (8) Tartarus database; (9) XMM/R. F. Mushotzky et al. 2008, in preparation; (10) EXOSAT/R. F. Mushotzky et al. 2008, in preparation; (11) Bassani et al. 1999; (12) BeppoSAX; (13) Matt et al. 2000; (14) Immler et al. 2003; (15) XMM; (16) Sambruna et al. 2006; (17) Gilli et al. 2000; (18) RXTE; (19) Maiolino et al. 1998; (20) XMM/Gondoin et al. 2003; (21) XMM/Perlmutter et al. 2005; (22) Chandra; (23) Risaliti et al. 1999; (24) Cappi et al. 2006; (25) Chandra/R. F. Mushotzky et al. 2008, in preparation; (26) ASCA; (27) Kennea et al. 2005; (28) Reynolds 1997; (29) Kraft et al. 2005; (30) Ballantyne 2005; (31) XRT/ Evans et al. 2006; (32) Ginga/Lawson & Turner 1997; (33) Véron-Cetty & Véron 2001; (34) Lewis et al. (2003; (35) no spectrum available; (36) Schoenmakers et al. 1998 ††; (37) 6dF ††; (38) Ueda et al. 2007; (39) Donzelli & Pastoriza 2000 ††; (40) Winter et al. 2008; (41) Sargent 1970; (42) SDSS ††; (43) Morelli et al. 2006; (44) Masetti et al. 2006; (45) Burenin et al. 2006; (46) SDSS—no AGN lines; (47) Giommi et al. 2005; (48) Halpern 2006; (49) Brinkmann et al. 1998; (50) Molina et al. 2006.

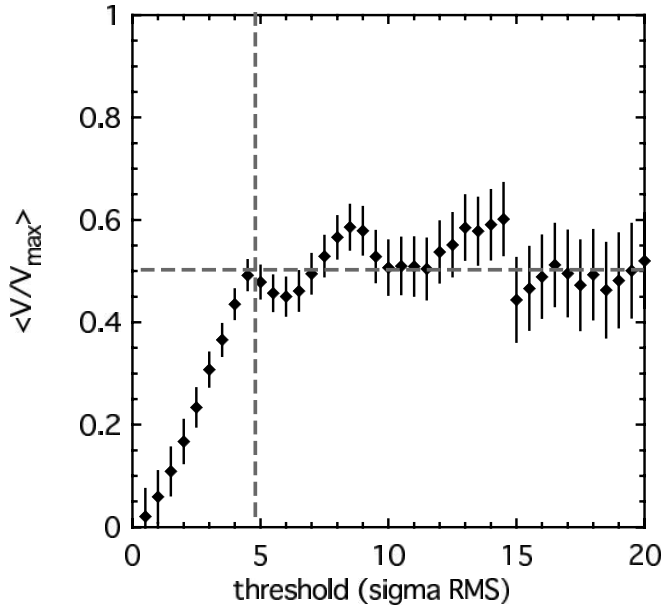


FIG. 4.—Plot of $\langle V/V_{\max} \rangle$ as a function of the significance threshold σ . For $\sigma > 4.5$ the average ratio is consistent with the nominal $\langle V/V_{\max} \rangle$ value of 0.5.

with an average n_{H} of 10^{22} . Using the Moretti et al. (2003) $\log N - \log S$ distribution based on *Chandra* data there are ~ 50 or 20 sources deg^{-2} , respectively, at these levels. Thus the probability of finding a detectable source falling by chance within a 2σ BAT error circle ($6'$ radius at threshold) is high. However most of these sources would be expected to have a very low flux in the BAT band and thus not be candidates for the counterparts of the BAT sources. We select the brightest source or sources at energies >3 keV as possible counterparts. A joint fit to the BAT and XRT data is performed using a simple spectral model (partially covered power law) and allowing the relative normalization between the BAT and XRT data to be a free parameter to

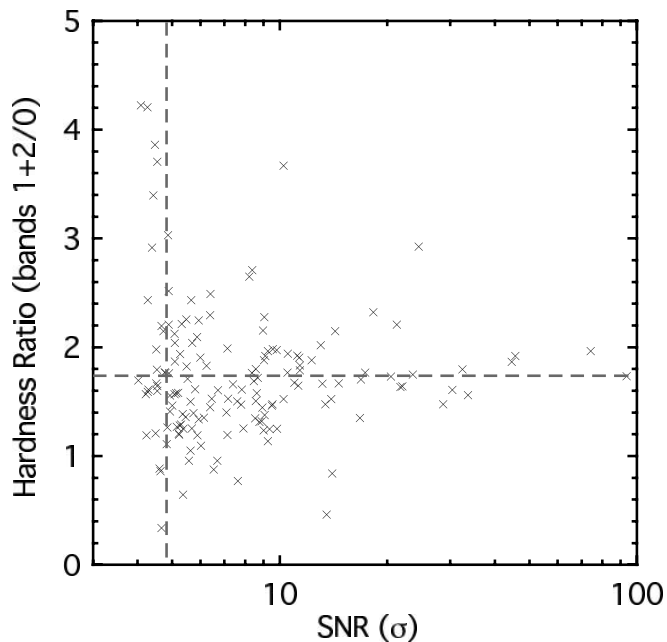


FIG. 5.—Hardness ratio [counts (25–100 keV)/counts (14–25 keV)] as a function of detection significance. There is no indication of discrimination against sources with soft spectra near the 4.8σ survey threshold.

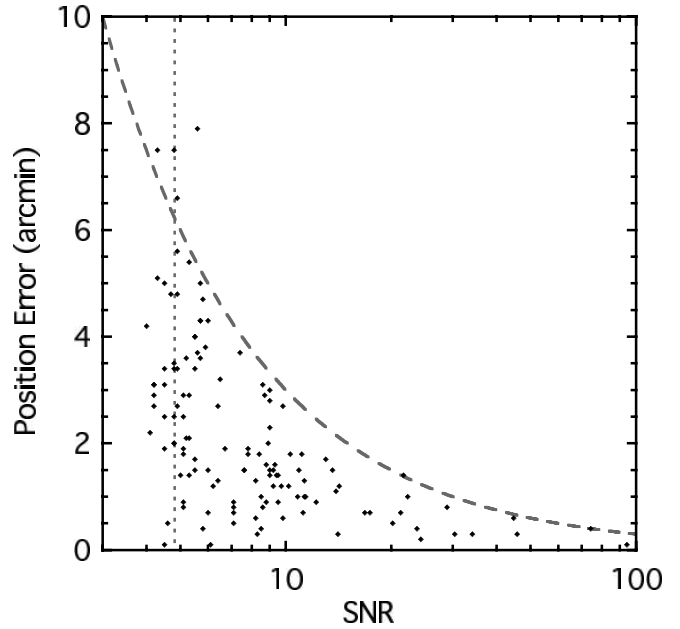


FIG. 6.—Distribution of mean offsets between positions measured with BAT and the counterpart as a function of the detection significance, SNR. The dashed line corresponds to $30/\text{SNR}$, or $6'$ at 5σ significance. The vertical dotted line is at the 4.8σ threshold used in this study. Sources below this threshold are not complete and have been identified because their known spectrum is consistent with the BAT result. Note that near the threshold the errors can occasionally be larger than this model predicts.

account for variability. Agreement is defined as a relative normalization factor <10 . A more complex model is not usually required because the XRT data have insufficient statistical significance to constrain complex models. See Winter et al. (2008) for a complete description. More complex models are required in a few cases where our sources have very high column densities or are Compton thick (L. M. Winter et al. 2008b, in preparation). These cases are flagged in the table as complex. We have used similar criteria for identifications based on archival data from other missions.

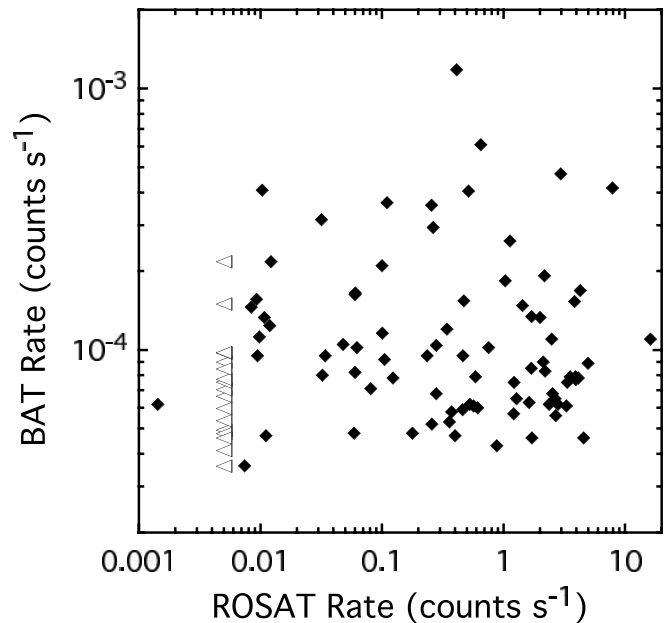


FIG. 7.—Comparison of *ROSAT* and BAT fluxes. Triangles indicate upper limits.

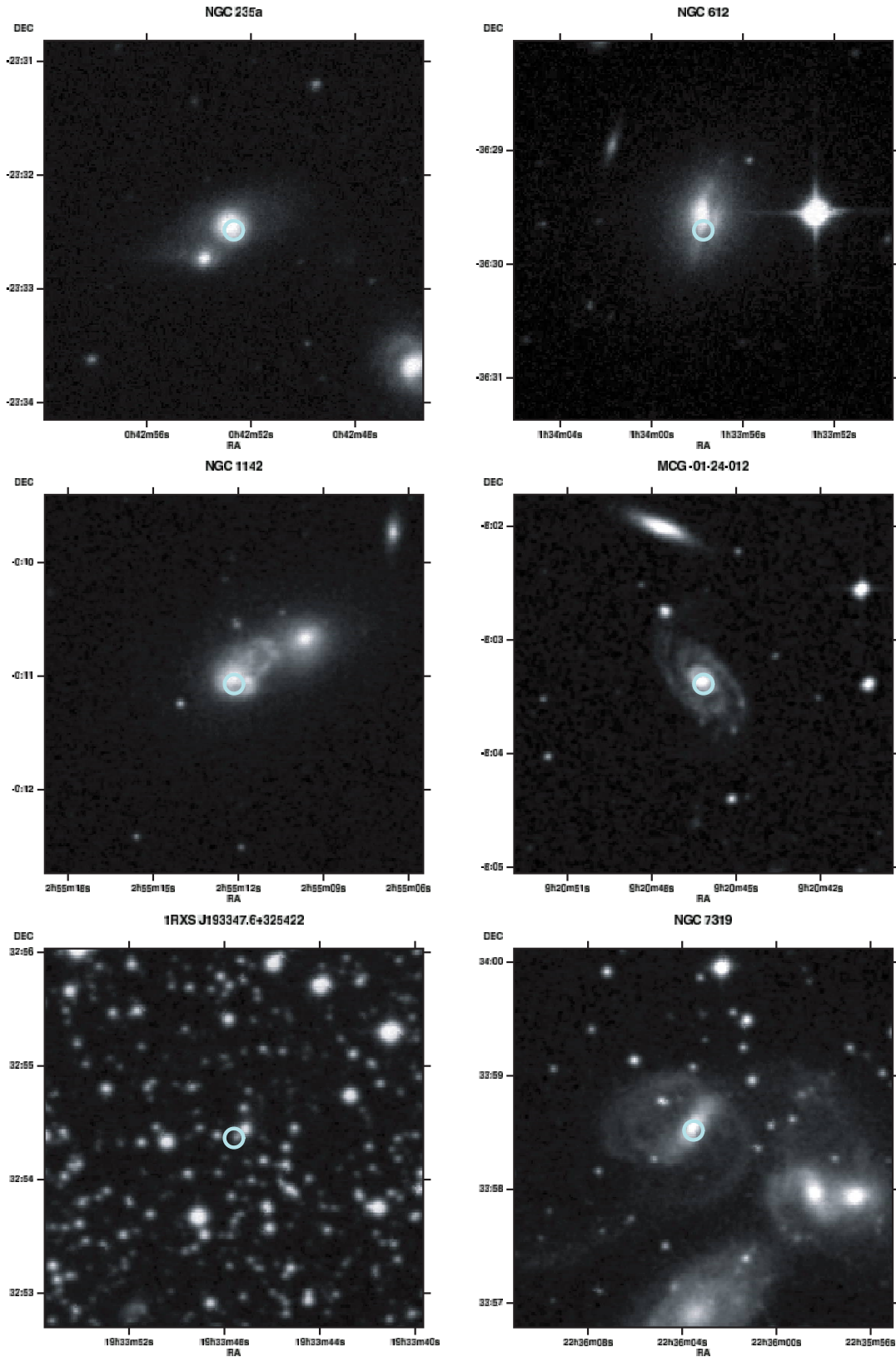


FIG. 8.—Examples of the optical counterparts and the XRT error circles for sources detected with BAT.

When an XRT counterpart has been found, the error circle radius is $\sim 4''$, and at the brightness of the optical counterparts (see below), there is a very high probability of identifying the object in 2MASS or DSS imaging data. For all but one of the $|b| > 15^\circ$ sources there is a redshift in the literature (based on

NED), or from our follow-up program (L. M. Winter et al. 2008b, in preparation) but often there is not an available optical spectrum. Thus a significant number of the objects do not have certain optical classifications. We have used the optical spectral types reported in Véron-Cetty & Véron (2006) for AGNs, where

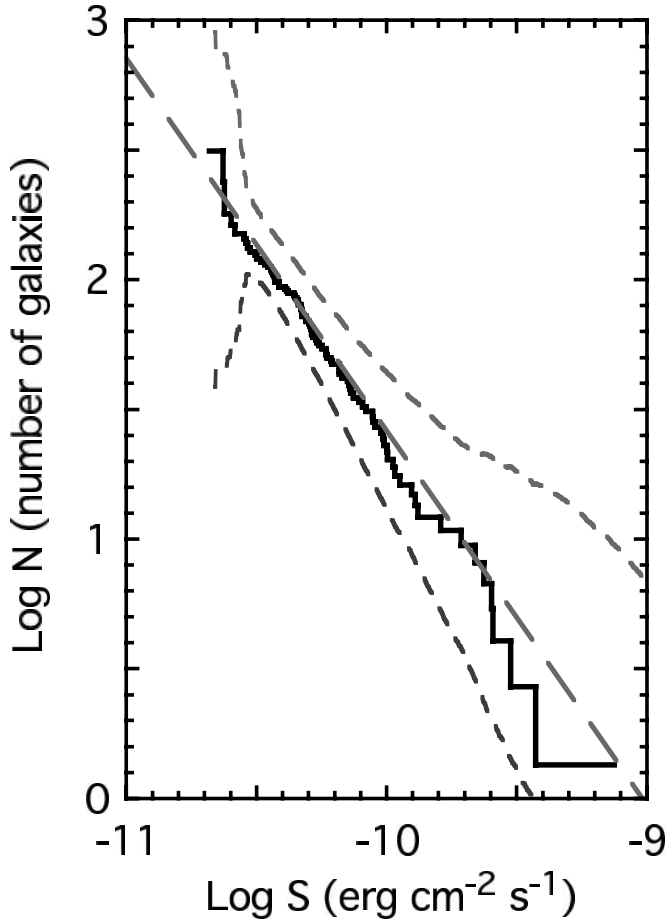


FIG. 9.—The $\log N$ – $\log S$ distribution for the BAT-selected AGNs. S is in units of $\text{erg cm}^{-2} \text{s}^{-1}$ in the energy range 14–195 keV. The short-dashed lines show the 99% confidence contours observed in Monte Carlo simulations of observations of sources with a constant space density, and the long-dashed lines a slope of -1.5 . The long-dashed line is derived from the best fit to the differential spectrum in Fig. 10.

available. In other cases we have used our own optical classifications based on SDSS or 6dF online data or what is available in NED and SIMBAD. We show in Figure 8 some of the optical counterparts and the XRT error circles.

With these criteria we have only one unidentified source out of 130 sources with $\sigma > 4.8$ and $|b| > 15^\circ$, but 13 out of 150 at $|b| < 15^\circ$. This difference arises from the much higher density of stars at lower Galactic latitudes and to the high degree of reddening and lack of large spectroscopic surveys in the Galactic plane. The relative completeness of the identifications in the BAT survey data contrasts with that of the *INTEGRAL* data (Masetti et al. 2006a; Bird et al. 2007) and is due to the extensive XRT follow-up and the accurate positions possible with the XRT. The one unidentified high-latitude source above 4.8σ , SWIFT J1657.3+4807, has no reasonable X-ray counterpart in the XRT field of view. Obvious possibilities are (1) that this source is a transient, or (2) that it has an extraordinarily high column density such that the flux in the 2–10 keV band is reduced by a factor of ~ 300 , e.g., a line-of-sight column density of $> 3 \times 10^{24} \text{ cm}^{-2}$, or a line-of-sight Compton optical depth of 2 (which would also require that there be no scattering into the line of sight greater than 0.2%), or (3) that it is a “false” source, of which we expect ~ 1 in the survey above our significance threshold.

We have examined the BAT light curves of all of the sources in Table 1 (including those below the 4.8σ threshold) and have

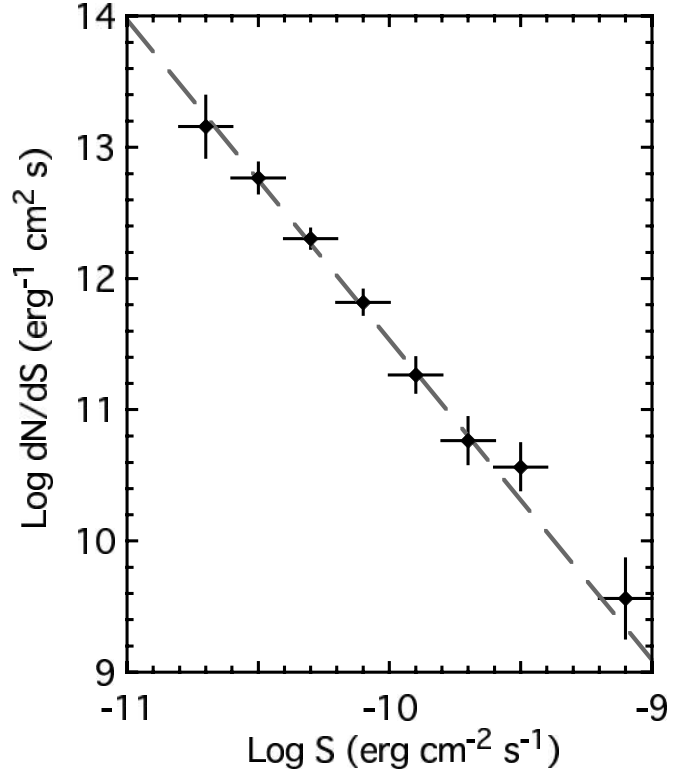


FIG. 10.—The differential $\log N$ – $\log S$ distribution corresponding to Fig. 9. The fitted line has a slope of -2.44 ± 0.14 .

determined that the sources SWIFT J0201.9–4513, SWIFT J0854.2+7221, SWIFT J1319.7–3350, and SWIFT J1328.4+6928 are almost certainly transients.

4. RESULTS

4.1. $\log N$ – $\log S$

When investigating the $\log N$ – $\log S$ law, correct allowance for sky coverage near the detection threshold is crucial. The sky coverage as a function of limiting flux that we have used (Fig. 1) was obtained using the same measured rms noise in the 9 month all-sky image that was used in assessing source significances. This direct measure of sky coverage is much more reliable than measures based on exposure as the systematic noise level varies across the sky and is not a simple function of exposure. At high fluxes the main uncertainties are due to Poisson statistics with a small number of objects. At low fluxes they are associated with the correction for completeness, which is a strong function of the flux, which is itself uncertain.

The $\log N$ – $\log S$ distribution (Figs. 9 and 10) is well fit by the standard $S^{-3/2}$ function for uniformly distributed sources and a normalization of 142.63 ± 9.864 AGNs with flux $> 3 \times 10^{-11} \text{ erg cm}^{-2} \text{ s}^{-1}$. Formally we find a slope of 1.42 ± 0.14 . Using a spectral slope for each object, we can compare this $\log N$ – $\log S$ law with those derived from *INTEGRAL* data (Beckmann et al. 2006b; Krivonos et al. 2005; Sazonov et al. 2007). Converting our $\log N$ – $\log S$ into the Sazonov et al. 17–60 keV band we find a normalization which is extremely close to their value. Conversion into the 20–40 keV band leads to a normalization of twice the Beckmann et al. value. The agreement with Sazonov et al. shows that the $\log N$ – $\log S$ law in the 14–195 keV band is now established to better than 15% accuracy. We do not understand the disagreement with Beckmann et al. and assume that it is due to the complex correction for sky coverage and the strong

TABLE 2
COMPARISON OF FITS TO THE AGN LUMINOSITY FUNCTION

| REFERENCE [$\log L_{14-195}$ (erg s $^{-1}$) = 44] | ENERGY BAND (keV) | L_* (erg s $^{-1}$) | | | |
|---|----------------------|------------------------|------------------------|-------------------------|-------------------------|
| | | a | b | Native Band | 14–195 keV |
| This work | 14–195 | $0.84^{+0.16}_{-0.22}$ | $2.55^{+0.43}_{-0.30}$ | ... | 43.85 ± 0.26 |
| Beckmann et al. (2006b) | 20–40 | 0.80 ± 0.15 | 2.11 ± 0.22 | 43.38 ± 0.35 | 43.99 ± 0.35 |
| Sazonov et al. (2007)..... | 17–60 | $0.76^{+0.18}_{-0.20}$ | $2.28^{+0.28}_{-0.22}$ | 43.40 ± 0.28 | 43.74 ± 0.28 |
| Barger et al. (2005)..... | 2–8 | 0.42 ± 0.06 | 2.2 ± 0.5 | 44.11 ± 0.08 | 44.54 ± 0.08 |
| La Franca et al. (2005)..... | 2–10 | $0.97^{+0.08}_{-0.10}$ | $2.36^{+0.13}_{-0.11}$ | 44.25 ± 0.18 | 44.61 ± 0.18 |
| Sazonov & Revnivtsev (2004) | 3–20 | $0.88^{+0.18}_{-0.20}$ | $2.24^{+0.22}_{-0.18}$ | $43.58^{+0.32}_{-0.30}$ | $43.83^{+0.32}_{-0.30}$ |

NOTES.—Luminosities have been converted to 14–195 keV values assuming a low energy slope of 1.7 breaking to 2.0 at 10 keV. Uncertainties do not take into account the uncertainty in the conversion. La Franca et al. quote a range of solutions; a representative one is used here. The normalization of the BAT AGN luminosity function A is $1.8^{+2.7}_{-1.1} \times 10^{-5}$ erg s $^{-1}$ Mpc $^{-3}$ at $\log L(\text{erg s}^{-1}) = 44$.

bias to previously known sources in the data set Beckmann et al. use. The Crab spectrum used by the Sazonov et al. group for *INTEGRAL* calibration is $10E^{-2.1}$ (see Churazov et al. [2007] for a detailed discussion of the use of the Crab Nebula as a calibrator). The BAT team uses $10E^{-2.15}$. In the 20–60 keV band the *INTEGRAL* normalization gives a Crab flux which is 1.15 higher. This would account for a normalization of the $\log N$ – $\log S$ law higher by a factor 1.23, consistent within the uncertainties. The closeness of the BAT sample introduces some uncertainty in the distance measurement due to the random velocities of galaxies (~ 500 km s $^{-1}$). To evaluate the effect of this uncertainty we have performed a Monte Carlo simulation of the luminosity function, including the uncertainty in luminosity and in distance due to the velocity error. This analysis indicates that the effect on the fitted parameters is $< 1 \sigma$. The break log luminosity could be 0.2 dex higher due to this error compared with a noise error of 0.4. The largest effect was on the high-luminosity slope which could be 0.3 larger due to systematics (error 0.35). These systematic errors do not substantially effect the *Swift* BAT luminosity function at its current statistical accuracy. Thus the $\log N$ – $\log S$ law in the 14–195 keV band is now established to $\sim 25\%$ accuracy; we know the number of sources quite accurately, but we do not know their flux to better than 15%.

4.2. Luminosity Function

The high identification completeness of our survey and the good understanding of the sky coverage are important in finding the luminosity function. We use the standard broken power law form

$$\frac{d\Phi(L_X)}{d \log L_X} = \frac{A}{(L_X/L_*)^a + (L_X/L_*)^b}, \quad (1)$$

This provides an excellent description of the data with the parameters given in Table 2. For comparison of other observations with ours we have converted luminosities quoted in other energy bands assuming a spectrum breaking from a slope of 1.7 to a slope of 2.0 at 10 keV. The BAT luminosity function shown in Figure 11 agrees well with those obtained by Beckman et al. (2006b) and by Sazonov et al. (2007) using data from *INTEGRAL* both in terms of the slopes and the break luminosities, although their errors are generally somewhat larger. However, we find a significantly lower break luminosity than found by Barger et al. (2005) and by La Franca et al. (2005) from observations at lower energies. The rather large difference cannot be caused by spectral conversion factors that neglect absorption in the 2–10 keV band, since this would make the observed 2–10 keV luminosity even lower

compared to the 14–195 keV value, exacerbating the problem. We thus believe that the disagreement between the luminosity functions is due to a deficit of objects at $\log L(\text{erg s}^{-1}) < 44.11$ in the 2–10 keV band. Considering that the bulk of the objects and their emitted luminosity lie near the break luminosity, this could imply a substantial modification to the present-day evolution models (e.g., Gilli et al. 2007).

As we show in the next section, the probability of an object being absorbed is a function of 14–195 keV luminosity. Hence there is a strong selection against detecting low-luminosity AGNs in softer X-ray surveys (see the discussion in Sazonov et al. 2007).

4.3. Nature of the Identifications

There are 151 sources in Table 1 which we have identified with AGNs. Of these, 102 are at high latitude ($|b| > 15^\circ$) and

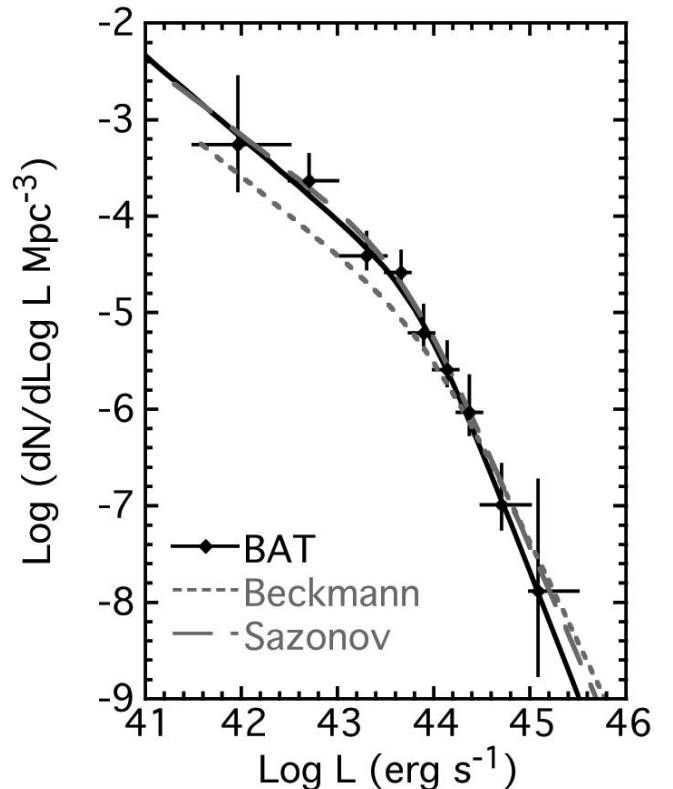


FIG. 11.—Comparison of the 14–195 keV luminosity function derived from the BAT observations with those found by Beckmann et al. (2006b) and by Sazonov et al. (2007) using *INTEGRAL*. The *INTEGRAL* luminosities have been converted to the BAT band assuming a power law with a photon index of 2.0.

above 4.8σ and form our complete sample. The remainder are at low latitude (42) and/or have lower significance in the final analysis (44). In the complete sample 14 out of 102 are beamed sources—BL Lac objects and blazars—(17 out of 152 overall) and the remainder are Seyferts and galaxies which show indications of activity. In addition, we have detected 32 Galactic sources and two galaxy clusters which meet the latitude and significance criteria for the complete sample. At low latitudes we also detect at $>4.8\sigma$ 103 Galactic sources, three galaxy clusters, and 13 unidentified sources. Although they are included in Table 1, we have not used sources identified as blazars or BL Lac objects, nor any source with $z > 0.5$, in the distribution functions.

We use the J -band magnitudes from the 2MASS survey to categorize the objects since that is the largest homogeneous database which covers the largest fraction of the *Swift* BAT sources. It is noticeable that the faintest optical counterparts are the blazars and the Galactic sources. The optically determined AGNs tend to be in fairly bright galaxies. One of the reasons that there are so few blazar identifications at low Galactic latitudes is the relative faintness of the likely optical counterparts combined with the lack of available redshifts and the effect of Galactic reddening.

Nine of the objects have not previously been optically classified as AGNs. An excellent example of this is the object NGC 4138 (Ho 1999; Moustakas & Kennicutt 2006) which shows little or no [O III] emission and in which only very high signal-to-noise ratio (SNR) spectra revealed a very faint broad $H\alpha$ line. Other objects, such as NGC 4102 (Moustakas & Kennicutt 2006), show no optical evidence of AGN activity.

For those objects which are optically classified as AGNs, 33 are Seyfert 1s, 14 are Seyfert 1.5s, and 35 are Seyfert 2s. There is reasonable but not perfect correlation between the optical classification and the presence of X-ray absorption (see below). Only two of 33 Seyfert 1s have a column density greater than 10^{22} cm^{-2} , whereas 4 of 14 Seyfert 1.5s and 33 of 35 Seyfert 2s are absorbed (two do not have X-ray column densities).

The median redshift of the nonblazars is ~ 0.017 . However, the blazar redshift distribution is very different with a long tail to high redshift and a median redshift of 0.24 (mean of 0.76). Thus we have been careful in determining the overall luminosity function to separate the blazars from the nonblazars since this will significantly change the slope of the high-luminosity end of the luminosity function.

4.4. X-Ray Spectral Analysis

The X-ray spectra of many of the sources have been published (see the references in Table 1). In these cases we have used the previously reported values of the column densities of the sources, while noting that the SNR of the observations varies greatly, as does the sophistication of the analysis and the type of models used to classify the spectra. Many of the spectra are rather complex (Winter et al. 2008), making assignment of errors to the column density difficult and highly model dependent. Where the column densities in Table 1 were obtained with *Swift* XRT follow-up observations, for homogeneity we report the results of simple absorbed power law fits. As shown in Figure 7, a large fraction of the BAT sources are not detected by the *ROSAT* all-sky survey, despite its factor of 100 better sensitivity for unabsorbed sources. This graphically illustrates the importance of obscuration in the selection of X-ray samples.

A detailed analysis of the archival *XMM*, *ASCA*, *BeppoSAX*, and *Chandra* data as well as the *Swift* XRT data is presented in another paper (Winter et al. 2008).

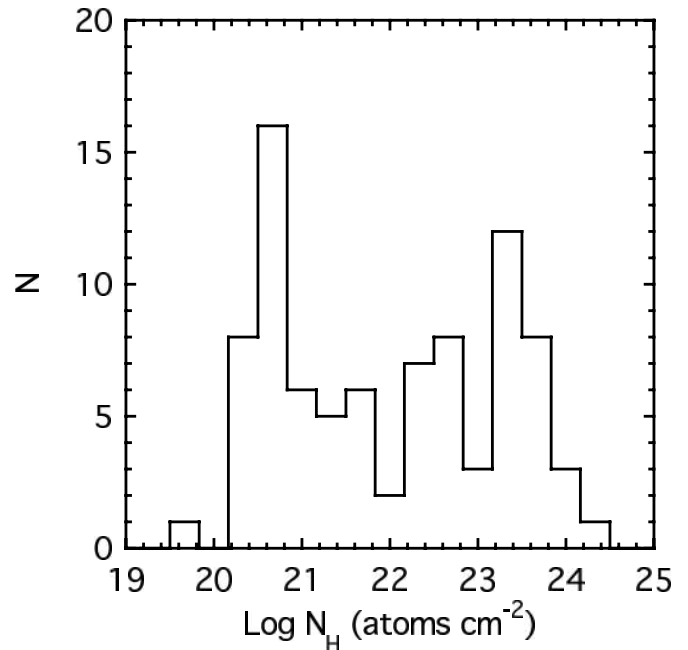


FIG. 12.—Distribution of column densities for the BAT-selected AGNs. Note the peak at low column densities and the relatively flat distribution above it. The Galactic column density has not been subtracted.

The distribution of absorption for the nonblazars (Fig. 12) is almost flat for $\log n_H(\text{cm}^{-2})$ in the range 21–24, with a strong peak at low column density due primarily to the effects of Galactic obscuration. The relative paucity of Compton-thick objects ($\log n_H[\text{cm}^{-2}] \geq 24.5$) is interesting. Unfortunately at such high columns the flux, even in the BAT energy band, is severely reduced so our level of completeness is uncertain. In addition we are only able to fit simplified models for many of these objects. Thus quantification of the lack of Compton-thick objects awaits more observations with high-sensitivity X-ray spectrometers (e.g., *XMM*, *Suzaku*).

As shown in Figure 13, the fraction of strongly absorbed AGNs drops with increasing luminosity. This is consistent with the previous claims of a drop in the absorbed fraction at higher luminosities, but it is not yet of sufficient statistical significance to confirm this dependence. While this has been seen in several X-ray-selected surveys (Ueda et al. 2003; La Franca et al. 2005; Shinozaki et al. 2006), the fact that the selection of BAT sources is independent of the line-of-sight column density confirms and extends these results.

4.5. BAT Spectral Analysis

At the present stage of analysis we only have four channel spectra available (this is a limitation of the present analysis software and is not intrinsic to the experiment). We have thus fit only simple power law models to the data.

The fact that the BAT hardness ratio shows no correlation with SNR (Fig. 5) indicates that there is no selection bias due to spectral parameters. The median spectral index is $\Gamma = 1.98$, in agreement with the *INTEGRAL* results from Beckmann et al. (2006b), with an rms spread 0.27. For a sample of 74 sources which have archival X-ray spectrum spectra at lower energies (e.g., Markowitz & Edelson 2004), the BAT slope is on average ~ 0.23 steeper than in the X-ray band (Fig. 14). A viable explanation for this (Nandra et al. 1999) is that the BAT data are detecting the “true” X-ray

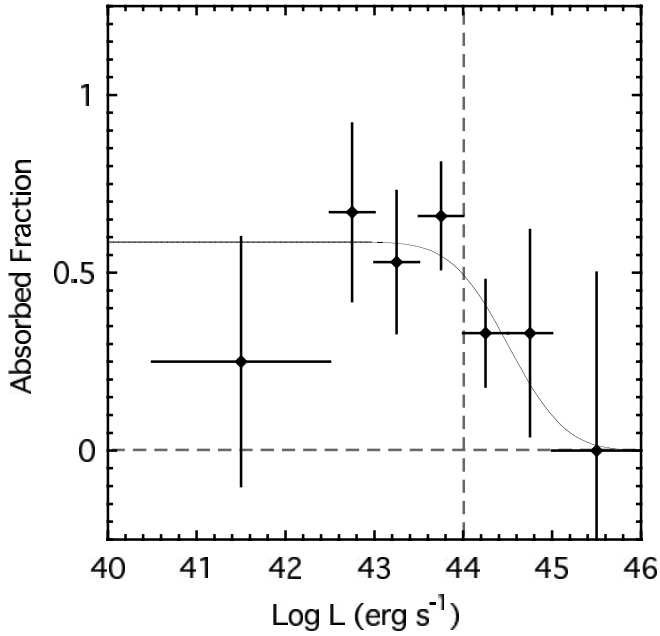


FIG. 13.—Fraction of BAT-selected AGNs with $n_{\text{H}} > 10^{22} \text{ cm}^{-2}$ as a function of 14–195 keV luminosity. The position of the break in the luminosity function slope is indicated. The smooth curve is simply one form which is consistent with the data. As elsewhere, only AGNs with $|b| > 15^\circ$ and significance greater than 4.8σ have been included. We note that if AGNs with $|b| < 15^\circ$ are included the drop at high luminosity is less pronounced, but it is still significant at the $>2 \sigma$ level.

spectral slope of 2, while the X-ray data are strongly influenced by the effects of reflection. Malizia et al. (2003) found using *BeppoSAX* hard X-ray data that Seyfert 2s are systematically harder than Seyfert 1s. A similar result is reported by Beckmann et al. (2006a). Comparison of the spectral index distributions of Seyfert 1s and Seyfert 2s (Fig. 15) confirms this finding;

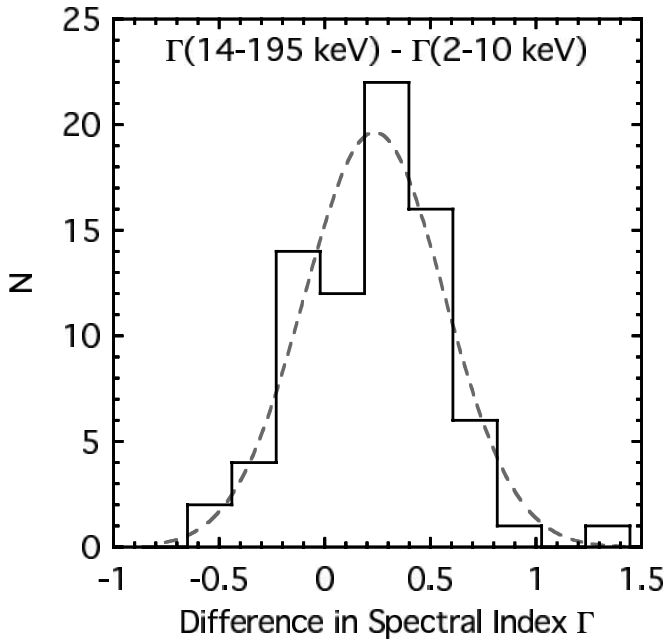


FIG. 14.—Histogram of the X-ray spectral index in the BAT band minus the X-ray spectral index. The X-ray indices are mostly from *ASCA* and *XRT* with some from various other missions. The mean difference is 0.26 with a standard deviation of 0.36.

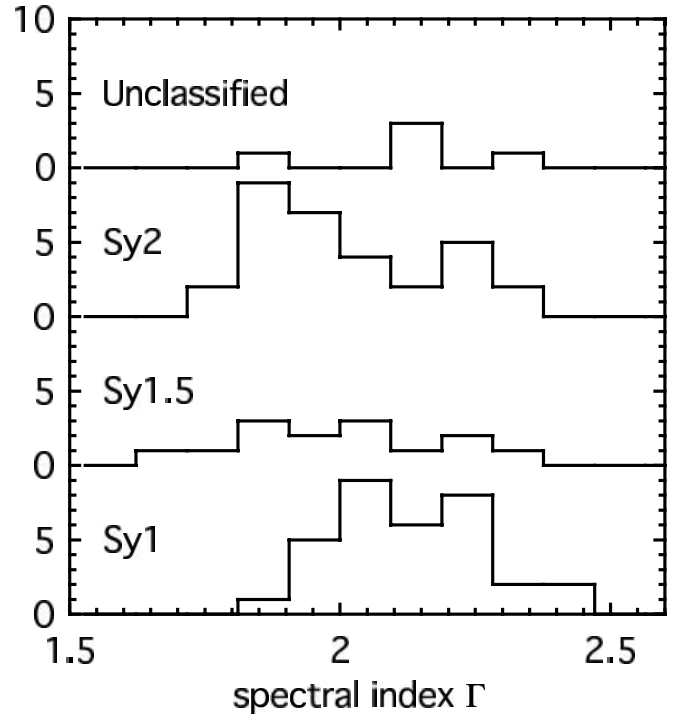


FIG. 15.—Distribution of power-law indices in the 14–195 keV band for BAT-selected sources sorted into Seyfert 1, Seyfert 1.5, Seyfert 2, and unclassified objects.

according to a Kolmogorov-Smirnov test the two distributions have a probability of less than 0.1% of arising from the same parent distribution function.

5. DISCUSSION

5.1. Luminosity Function

As shown above the low-luminosity slope of the luminosity function of hard X-ray selected AGNs is steeper than that of the 2–8 keV function of Barger et al. (2005). We believe that this is due to the high fraction of heavily absorbed objects at low BAT luminosities. Thus the contribution of low-luminosity objects to the 10–100 keV background is larger than originally calculated. This is confirmed by the agreement of the slope of our luminosity function with the absorption-corrected low-luminosity slope of La Franca et al. (2005), which unlike Barger et al. (2005) assumes an absorption that depends on luminosity. The break in the luminosity function is quite robust and thus is an intrinsic feature of the luminosity function and is not due to a spectral selection effect. Integration of our luminosity function gives a local volume density of $n(L_X > 10^{41} \text{ erg s}^{-1}) = 2.4 \times 10^{-3} \text{ Mpc}^{-3}$, compared to a density of 0.02 Mpc^{-3} galaxies brighter than $M_* = -19.75$ (Cross et al. 2001), and a local emissivity of $2.3 \times 10^{39} \text{ erg s}^{-1} \text{ Mpc}^{-3}$. The choice of M_* defines the location of the knee in the luminosity function and is the typical absolute magnitude for a galaxy. It is a simple way of estimating the galaxy density. The typical *J*-band absolute magnitude at the knee is $M_* = -21.73$ (Cole et al. 2001). The median BAT *J*-band absolute magnitude is $M = -23.8$ and only three BAT AGNs have $M > -22$. Hence $\approx 10\%$ of luminous galaxies in the local universe are AGNs with a hard X-ray luminosity $\geq 10^{41} \text{ erg s}^{-1}$. Because of the low median redshift of the sample, the BAT data are not sensitive to evolution in the luminosity function and $V/V_{\text{max}} \sim 0.5$ is as expected.

5.2. $\log N$ – $\log S$

There have been numerous predictions of the hard X-ray $\log N$ – $\log S$ (Treister et al. 2006; Gandhi & Fabian 2003) and our data allow a direct comparison of these models. Converting the observed BAT $\log N$ – $\log S$ to the band predicted by these authors, we find that we have good agreement with the predictions of Gandhi et al. (2004), but lie a factor of 2 lower than the predictions of Treister et al. (2006). Since each of these models makes different assumptions, our hard X-ray survey should be able to determine which are valid.

5.3. The Distribution of n_H

In Figures 13 and 15 the distribution of column densities over all objects is almost flat and appears to depend on hard X-ray luminosity. Similar results based on the *RXTE* slew survey were obtained by Sazonov & Revnivtsev (2004). The standard unified model predicts that the ratio of absorbed to unabsorbed objects should be 4:1, as opposed to our observed value of 1:1. This difference is probably due to the neglect of the luminosity dependence of absorption in the simple unified model. The BAT results are roughly consistent with dependence of absorption on luminosity seen previously (Ueda et al. 2003; Steffen et al. 2003; Gilli et al. 2007). We note that the distribution of column densities in Tozzi et al. (2006) from the *Chandra* deep fields is rather different from the BAT sample in that the Tozzi et al. sample seems to be missing the low n_H half of the distribution. This has been confirmed by Wang et al. (2007) and by Gilli et al. (2007). Direct comparison of the n_H distribution from the BAT sample and Tozzi et al. shows apparent differences, especially at low n_H . Taken at face value, this would indicate an evolution of the n_H distribution between the low median redshift of the BAT sample (0.03) and the redshift of the Tozzi sample (~ 0.7). This is similar to the results reported by La Franca et al. (2005); however, Hasinger et al. (2007) find no such dependence.

6. CONCLUSION

We have presented the results of an AGN survey using data from the BAT instrument on *Swift*. The use of a hard X-ray bandpass means that the survey is immune to the effects of X-ray absorption that have traditionally plagued similar studies in optical and soft X-ray bandpasses, raising serious questions concerning completeness. Utilizing the standard AGN broken power law prescription to characterize the differential luminosity distribution function, we find that the data can be very well described taking a break luminosity $\log L_* (\text{erg s}^{-1}) = 43.85 \pm 0.26$, a low-luminosity power law slope $a = 0.84^{+0.16}_{-0.22}$, and a high-luminosity power law slope $b = 2.55^{+0.43}_{-0.30}$, in agreement with other studies based on hard X-ray survey data such as that of Sazonov et al. (2007) using *INTEGRAL*. We find a median spectral index 1.98, in accord with the Beckmann et al. (2006b) study using *INTEGRAL*. By

integrating our inferred luminosity function above $10^{41} \text{ erg s}^{-1}$, we arrive at a local volume density of $2.4 \times 10^{-3} \text{ Mpc}^{-3}$, roughly 10% of the local density of luminous galaxies.

The BAT survey has detected 31 AGNs at $>4.8 \sigma$ that were not previously detected in hard X-rays, of which nine were not previously identified as AGNs by other techniques. In addition, there are 14 BAT AGNs that were also detected contemporaneously in hard X-rays by *INTEGRAL*, of which five had not been previously identified as AGNs. For sources that were detected by both instruments, there is a good correlation between the BAT and *INTEGRAL* flux, with the exception of a few sources that are almost certainly variable. There are 42 *INTEGRAL* AGNs with $\text{SNR} > 4.8$ that were not detected by BAT. Only 11 of these have a flux (scaled to the BAT energy band assuming E^{-2} spectrum) that is greater than $3 \times 10^{-11} \text{ erg cm}^{-2} \text{ s}^{-1}$, where a BAT detection is likely. Most of these high-flux, undetected sources are within 30° of the Galactic center, where the BAT survey has significantly reduced sensitivity due to lower exposure and increased systematic errors. Of the BAT detected sources, 13% were not previously known to be AGNs.

With increased exposure, both the BAT and *INTEGRAL* survey sensitivities will improve, and we expect most of the new unidentified hard X-ray sources to be in the interesting class of very heavily absorbed AGNs. *INTEGRAL* detected 111 AGNs at $>4.8 \sigma$ in ~ 4 yr. Due to its larger FOV and random observing strategy, BAT detected 126 AGNs in 0.75 yr, a rate 6 times faster than *INTEGRAL*. We expect both missions to continue accumulating new AGNs at the same rates, in which case BAT AGNs will become an increasing fraction of the new detections. At 3 yr after the *Swift* launch, we predict 450 BAT-detected AGNs and more than 60 that not have been previously identified as AGNs. The hard X-ray measurements are unique in another sense. We believe they yield an accurate measurement of the average luminosity of these sources. We have shown (L. M. Winter et al. 2008a and 2008b, in preparation) that the luminosity and power-law index for absorbed sources cannot be accurately derived from 2–10 keV X-ray measurements alone, even with *XMM* or *Chandra*. For the $\sim 1/2$ of all AGNs that are absorbed, the BAT and *INTEGRAL* surveys provide unique new measurements of the luminosity and underlying power law.

This is the second paper in a series. In future papers we will present the X-ray spectral properties of these objects, the long-term BAT light curves, detailed spectral analysis of the BAT data, and the optical properties of the hosts of the BAT sources, and extend the sample by a factor of 2 in size.

We gratefully acknowledge the help of Stephane Paltani, whose careful checking of our preprint uncovered an error in our plotting of *INTEGRAL* data.

REFERENCES

- Akylas, A., Georgantopoulos, I., Griffiths, R. G., Papadakis, I. E., Mastichiadis, A., Warwick, R. S., Nandra, K., & Smith, D. A. 2002, *MNRAS*, 332, L23
 Alexander, D. M., et al. 2003, *AJ*, 126, 539
 Alonso-Herrero, A., et al. 2006, *ApJ*, 640, 167
 Ballantyne, D. R. 2005, *MNRAS*, 362, 1183
 Barger, A. J., Cowie, L. L., Mushotzky, R. F., & Richards, E. A. 2001, *AJ*, 121, 662
 Barger, A. J., Cowie, L. L., Mushotzky, R. F., Yang, Y., Wang, W.-H., Steffen, A. T., & Capak, P. 2005, *AJ*, 129, 578
 Barger, A. J., et al. 2003, *AJ*, 126, 632
 Barmby, P., et al. 2006, *ApJ*, 642, 126
 Barthelmy, S. D., et al. 2005, *Space Sci. Rev.*, 120, 143
 Bassani, L., Dadina, M., Maiolino, R., Salvati, M., Risaliti, G., della Cecca, R., Matt, G., & Zamorani, G. 1999, *ApJS*, 121, 473
 Beckmann, V., Gehrels, N., Shrader, C. R., & Soldi, S. 2006a, *ApJ*, 638, 642
 Beckmann, V., Soldi, S., Shrader, C. R., Gehrels, N., & Produit, N. 2006b, *ApJ*, 652, 126
 Bird, A. J., et al. 2007, *ApJS*, 170, 175
 Brandt, W. N., & Hasinger, G. 2005, *ARA&A*, 43, 827
 Brinkmann, W., Otani, C., Wagner, S. J., & Siebert, J. 1998, *A&A*, 330, 67
 Burenin, R., Meshcheryakov, A., Revnivtsev, M., Bikmaev, I., & Sunyaev, R. 2006, *ATel*, 880, 1
 Cappi, M., et al. 2006, *A&A*, 446, 459
 Churazov, E., et al. 2007, *A&A*, 467, 529
 Cole, S., et al. 2001, *MNRAS*, 326, 255
 Cross, N., et al. 2001, *MNRAS*, 324, 825
 Donzelli, C. J., & Pastoriza, M. G. 2000, *AJ*, 120, 189

- Evans, D. A., Worrall, D. M., Hardcastle, M. J., Kraft, R. P., & Birkinshaw, M. 2006, *ApJ*, 642, 96
- Franceschini, A., et al. 2006, *A&A*, 453, 397
- Gallo, L. C., Lehmann, I., Pietsch, W., Boller, T., Brinkmann, W., Friedrich, P., & Grupe, D. 2006, *MNRAS*, 365, 688
- Gandhi, P., Crawford, C. S., Fabian, A. C., & Johnstone, R. M. 2004, *MNRAS*, 348, 529
- Gandhi, P., & Fabian, A. C. 2003, *MNRAS*, 339, 1095
- Gehrels, N., et al. 2004, *ApJ*, 611, 1005
- Giacconi, R., et al. 2002, *ApJS*, 139, 369
- Gilli, R., Comastri, A., & Hasinger, G. 2007, *A&A*, 463, 79
- Gilli, R., Maiolino, R., Marconi, A., Risaliti, G., Dadina, M., Weaver, K. A., & Colbert, E. J. M. 2000, *A&A*, 355, 485
- Giommi, P., Piranomonte, S., Perri, M., & Padovani, P. 2005, *A&A*, 434, 385
- Gondoin, P., Orr, A., Lumb, D., & Siddiqui, H. 2003, *A&A*, 397, 883
- Gruber, D. E., Matteson, J. L., Peterson, L. E., & Jung, G. V. 1999, *ApJ*, 520, 124
- Halpern, J. P. 2006, *ATel*, 847, 1
- Hasinger, G., et al. 2007, *ApJS*, 172, 29
- Heckman, T. M., Ptak, A., Hornschemeier, A., & Kauffmann, G. 2005, *ApJ*, 634, 161
- Ho, L. C. 1999, *ApJ*, 516, 672
- Immler, S., Brandt, W. N., Vignali, C., Bauer, F. E., Crenshaw, D. M., Feldmeier, J. J., & Kraemer, S. B. 2003, *AJ*, 126, 153
- Kennea, J. A., et al. 2005, *ATel*, 677, 1
- Kraft, R. P., Hardcastle, M. J., Worrall, D. M., & Murray, S. S. 2005, *ApJ*, 622, 149
- Krivonos, R., Vikhlinin, A., Churazov, E., Lutovinov, A., Molkov, S., & Sunyaev, R. 2005, *ApJ*, 625, 89
- La Franca, F., et al. 2005, *ApJ*, 635, 864
- Lawson, A. J., & Turner, M. J. L. 1997, *MNRAS*, 288, 920
- Levine, A. M., et al. 1984, *ApJS*, 54, 581
- Lewis, K. T., Eracleous, M., & Sambruna, R. M. 2003, *ApJ*, 593, 115
- Lutz, D., Maiolino, R., Spoon, H. W. W., & Moorwood, A. F. M. 2004, *A&A*, 418, 465
- Mainieri, V., Bergeron, J., Hasinger, G., Lehmann, L., Rosati, P., Schmidt, M., Szokoly, G., & Della Ceca, R. 2002, *A&A*, 393, 425
- Mainieri, V., et al. 2005, *A&A*, 437, 805
- Maiolino, R., Salvati, M., Bassani, L., Dadina, M., della Ceca, R., Matt, G., Risaliti, G., & Zamorani, G. 1998, *A&A*, 338, 781
- Malizia, A., Bassani, L., Stephen, J. B., Di Cocco, G., Fiore, F., & Dean, A. J. 2003, *ApJ*, 589, L17
- Markowitz, A., & Edelson, R. 2004, *ApJ*, 617, 939
- Markwardt, C. B., Tueller, J., Skinner, G. K., Gehrels, N., Barthelmy, S. D., & Mushotzky, R. F. 2005, *ApJ*, 633, L77
- Masetti, N., et al. 2006a, *A&A*, 448, 547
- . 2006b, *A&A*, 459, 21
- Matt, G., Fabian, A. C., Guainazzi, M., Iwasawa, K., Bassani, L., & Malaguti, G. 2000, *MNRAS*, 318, 173
- Meléndez, M., et al. 2008, *ApJ*, in press (arXiv:0804.1147)
- Molina, M., et al. 2006, *MNRAS*, 371, 821
- Morelli, L., Masetti, N., Bassani, L., Landi, R., Malizia, A., Bird, A. J., Ubertini, P., & Galaz, G. 2006, *ATel*, 785, 1
- Moretti, A., Campana, S., Lazzati, D., & Tagliaferri, G. 2003, *ApJ*, 588, 696
- Moustakas, J., & Kennicutt, Jr., R. C. 2006, *ApJS*, 164, 81
- Nandra, K., George, I. M., Mushotzky, R. F., Turner, T. J., & Yaqoob, T. 1999, *ApJ*, 523, L17
- Perlman, E. S., et al. 2005, *ApJ*, 625, 727
- Predehl, P., & Schmitt, J. H. M. M. 1995, *A&A*, 293, 889
- Reynolds, C. S. 1997, *MNRAS*, 286, 513
- Risaliti, G., Maiolino, R., & Salvati, M. 1999, *ApJ*, 522, 157
- Sambruna, R. M., George, I. M., Mushotzky, R. F., Nandra, K., & Turner, T. J. 1998, *ApJ*, 495, 749
- Sambruna, R. M., et al. 2006, *ApJ*, 646, 23
- Sargent, W. L. W. 1970, *ApJ*, 159, 765
- Sazonov, S., Churazov, E., Revnivtsev, M., Vikhlinin, A., & Sunyaev, R. 2005, *A&A*, 444, L37
- Sazonov, S., & Revnivtsev, M. 2004, *A&A*, 423, 469
- Sazonov, S., Revnivtsev, M., Krivonos, R., Churazov, E., & Sunyaev, R. 2007, *A&A*, 462, 57
- Schoenmakers, A. P., Mack, K.-H., Lara, L., Roettgering, H. J. A., de Bruyn, A. G., van der Laan, H., & Giovannini, G. 1998, *A&A*, 336, 455
- Schwope, A., et al. 2000, *Astron. Nachr.*, 321, 1
- Shinozaki, K., Miyaji, T., Ishisaki, Y., Ueda, Y., & Ogasaka, Y. 2006, *AJ*, 131, 2843
- Steffen, A. T., Barger, A. J., Cowie, L. L., Mushotzky, R. F., & Yang, Y. 2003, *ApJ*, 596, L23
- Stern, D., et al. 2005, *ApJ*, 631, 163
- Szokoly, G. P., et al. 2004, *ApJS*, 155, 271
- Tozzi, P., et al. 2006, *A&A*, 451, 457
- Treister, E., et al. 2005, *ApJ*, 621, 104
- . 2006, *ApJ*, 640, 603
- Ueda, Y., Akiyama, M., Ohta, K., & Miyaji, T. 2003, *ApJ*, 598, 886
- Ueda, Y., et al. 2007, *ApJ*, 664, L79
- Véron-Cetty, M.-P., & Véron, P. 2006, *A&A*, 455, 773
- Voges, W., et al. 1999, *A&A*, 349, 389
- Wang, J. X., et al. 2007, *ApJ*, 657, 95
- Watanabe, C., Ohta, K., Akiyama, M., & Ueda, Y. 2004, *ApJ*, 610, 128
- Weedman, D., et al. 2006, *ApJ*, 653, 101
- Winter, L. M., et al. 2008, *ApJ*, 674, 686
- Worsley, M. A., et al. 2005, *MNRAS*, 357, 1281
- Yang, Y., Mushotzky, R. F., Steffen, A. T., Barger, A. J., & Cowie, L. L. 2004, *AJ*, 128, 1501
- Zheng, W., et al. 2004, *ApJS*, 155, 73